

Type of the Paper (Editorial)

## 3D Printing in Dentistry – Discovering New Possibilities

Tamer M. Hamdy <sup>1,\*</sup>

<sup>1</sup> Restorative and Dental Materials Department, Oral and Dental Research Institute, National Research Centre (NRC), Giza, Dokki, 12622, Egypt

\* Corresponding author e-mail: [dr\\_tamer\\_hamdy@yahoo.com](mailto:dr_tamer_hamdy@yahoo.com)

**Citation:** Tamer M. Hamdy. 3D Printing in Dentistry – Discovering New Possibilities. *Biomat. J.*, 3 (1),1 – 2 (2024).

<https://doi.org/10.5281/znodo.5829408>

Received: 19 December 2024

Accepted: 20 December 2024

Published: 25 December 2024



**Copyright:** © 2022 by the authors. Submitted for possible open access publication under the terms and conditions of the Creative Commons Attribution (CC BY) license (<https://creativecommons.org/licenses/by/4.0/>).

**Abstract:** 3D printing is often regarded as a groundbreaking technology that is set to transform the manufacturing landscape. Its applications span across various fields, including aerospace, defense, art, and design, but it is gaining particular traction in the realm of surgery. The technology is especially relevant in dentistry, where advancements in 3D imaging and modeling technologies, such as cone beam computed tomography and intraoral scanning, are making a significant impact. Coupled with the established use of CAD CAM technologies in the dental field, 3D printing is poised to play an increasingly vital role. Some of its applications include creating drill guides for dental implants, producing physical models for prosthodontics, orthodontics, and surgical procedures, manufacturing dental, craniomaxillofacial, and orthopedic implants, as well as fabricating copings and frameworks for dental restorations. This paper explores the various types of 3D printing technologies available and their diverse applications in dentistry and maxillofacial surgery.

**Keywords:** 3D Printing; digital dentistry; dental material

The profession has embraced digital manufacturing technologies, transforming much of the laboratory work that was once done by artisans into digital processes. Now, only the final touches of restorations are applied by hand. CAD CAM technology has become a standard in dental laboratories and is increasingly being integrated into dental surgeries. In the past, scanning and the creation of digitally manufactured restorations depended on centralized facilities, but many laboratories now possess their own scanners and milling units. In dental practices, intraoral and CBCT scanners are becoming increasingly prevalent.

As a result, dentists and dental technicians are becoming familiar with handling large amounts of digital data. 3D printing serves as another output option for dental CAD software, allowing for the creation of complex components and objects from various materials. It is particularly beneficial for unique, custom structures with intricate designs, especially when 3D scan data is readily available.

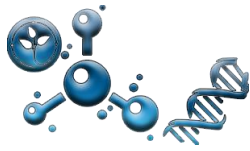
In the field of dentistry, 3D printing has a wide range of applications and holds significant potential for enabling innovative treatments and manufacturing methods for dental restorations. While national regulatory bodies have yet to establish guidelines for the use of 3D printing in surgery or dentistry, there will eventually be a need for regulators to address this technology and set appropriate standards.

Despite 3D printing technologies being accessible for over a decade, it is advancements in scanner technology, computer-aided design software, and increased computational power that have made the practical use of this technology feasible. Additionally, growing commercial and public interest has heightened awareness and improved access to necessary resources.

With the advent of milling technology, a wide array of new materials became accessible for creating restorations; likewise, new generations of dental restorative materials for 3D printing are continuously being developed and introduced. Considering

the various applications of 3D printing in dentistry, along with the profession's extensive experience with scanning and milling technology, it can be argued that dentists and dental technologists possess more experience with these 3D manufacturing technologies than any other field. While CAD software remains primarily in the hands of those who are well-trained and tech-savvy, this will not deter newer generations of operators, as the software is constantly evolving to become more intuitive and user-friendly. Significant future advancements that could enhance our use of this technology, beyond the clear advantages of lower costs, faster production times, and more efficient, less invasive treatments for patients, include the ability to 3D print with ceramic materials featuring digital coloration and staining, minimizing the post-processing required for metal components, and incorporating machining/milling of 3D printed metal parts into the overall metal printing process.

The gradual integration of digital technologies in dentistry has gained significant traction, leading the authors to believe that we have moved well beyond the early adoption phase. We now have a real opportunity for the widespread use of 3D printing technology in orthodontics, dental laboratories, and surgical practices. There is immense potential for further advancements; while much attention is given to individual pieces of equipment, the crucial factor lies in how well these tools integrate with planning and design software. This integration is essential for creating a seamless, efficient workflow, which will ultimately influence the acceptance and implementation of these transformative technologies. With the advent of this new technology comes a wealth of opportunities. The challenge we face is to view 3D printing not merely as a new tool for traditional practices, but as a means to foster creativity, develop innovative materials, and establish more predictable, less invasive, and cost-effective procedures for our patients. We must also be cautious not to fall into the trap of assuming that digital solutions are inherently superior. Research is essential to establish standards and ensure that the rapidly emerging equipment in our laboratories and surgeries performs at least as effectively as existing conventional 'analog' methods.



Type of the Paper (Research Article)

## Knowledge and Attitude Regarding Designing Removable Partial Denture Among Interns and Dental Students; Dental Schools in Benghazi \ Libya

SUAD A. ALMASALATI<sup>1</sup>, Hana E. Mahjoub<sup>2</sup>, Khadiga I. Elfallah<sup>3</sup>, Sara Mohamed.A.M. Bogazia<sup>4</sup>

**Citation:** SUAD A. ALMASALATI, Hana E. Mahjoub, Khadiga I. Elfallah, Sara Mohamed.A.M. Bogazia. Knowledge and Attitude Regarding Designing Removable Partial Denture Among Interns and Dental Students; Dental Schools in Benghazi \ Libya. *Biomat. J.*, 3 (1), 3 – 13 (2024).

<https://doi.org/10.5281/znodo.5829408>

Received: 10 December 2024

Accepted: 24 December 2024

Published: 25 December 2024



**Copyright:** © 2023 by the authors. Submitted for possible open access publication under the terms and conditions of the Creative Commons Attribution (CC BY) license (<https://creativecommons.org/licenses/by/4.0/>).

<sup>1</sup> Assistant lecturer, Department of Removable Prosthodontics, Faculty of Dentistry, University of Benghazi, Benghazi, Libya

<sup>2</sup> Assistant professor, Department of Removable Prosthodontics, Faculty of Dentistry, University of Benghazi, Benghazi, Libya

<sup>3</sup> Lecturer, Department of fixed Prosthodontics, Faculty of Dentistry, University of Benghazi, Benghazi, Libya

<sup>4</sup> Assistant lecturer, Department of oral biology, Faculty of Dentistry, Ajdabia University, Ajdabia, Libya

\* Corresponding author e-mail: [Lady.dent@yahoo.com](mailto:Lady.dent@yahoo.com)

**Abstract:** A removable partial denture is an economical and reversible treatment option thus it is considered as one of the most successful treatment options for partially edentulous patients. The aim of this study was To evaluate the Knowledge and Attitude of undergraduate students and interns in providing proper design of Removable Partial denture (RPD) to Patients in dental schools of Benghazi \ Libya, to improve the undergraduate curriculum that can be beneficial for the newly graduating student and the practicing dentist. Materials and methods : A cross-sectional study design was conducted among dental students and interns at the Faculties of Dentistry of both the University of Benghazi and LIMU. Results : One hundred and thirty registered dentists completed the questionnaire, It was revealed that half (50%) of participants reported never providing RPD service. The majority (63.8%), indicated that they communicate with the laboratory by both marking on the primary cast and laboratory form. less than half (40.8%) of respondents reported that they survey all the time. Almost half (48.5%) reported that their dental technician follows their design instructions. A significant portion of participants (61.5%) believe that designing an RPD is the responsibility of the dentist, The majority of respondents review their basic knowledge before starting an RPD design following the ADA guidelines. Conclusion : Within the limitation of this study we can conclude that; our dental students in both universities (Benghazi and LIMU) have less chance to practice RPD at dental schools On other hand, showed acceptable level of knowledge about designing of RPD. Further practice is recommended.

---

**Keywords:** *Knowledge, Attitude, Designing, Removable partial denture RPD*

---

## 1. Introduction

Awareness of the dental health was markedly increased, therefore the incidence of edentulism also declined but the number of edentulous individuals remains high due to the population increase[1]. Prosthetic reconstruction of completely or partially edentulous arches is needed as edentulism is considered as disability according to World Health Organization (WHO). A progressive decrease in complete denture wearers and increase of partial denture wearers were noticed due to preservation of the remaining natural teeth which was enforced by recent trained in dentistry. The treatment modalities of partial edentulism include various solutions like removable partial denture, fixed partial prosthesis, and implant assisted prosthesis[2]. A removable partial denture is an economical and reversible treatment option thus it is considered as one of the most successful treatment options for partially edentulous patients[3]. A proper RPD construction requires clinical and laboratory steps that include proper diagnosis and treatment planning, primary impression, survey of the primary cast, initial designing of the prosthesis on the cast, prosthetic mouth preparation, secondary impression, and secondary cast reorientation on the dental surveyor to check the amount of performed teeth modification. There are several components of an RPD each component has a function. Thus, dentists should have clear knowledge regarding design of the various components of the RPD structure. The final design is drawn up and submitted to the laboratory technician to follow the design instructions[4]. Successful communication between dentist and dental technicians is required to fabricate a proper prosthesis, but proper designing of RPD is the responsibility of dentist and is not the job of the technician[5]. An interactive relationship between dentists and dental technicians is required for achieving a successful outcome as there is an increase in the patient's knowledge and needs. Clear effective communication of design features between dental practitioners and dental technicians is a main factor for the production of high quality fixed and removable prostheses[6,7].

Low patient satisfaction with major biological and mechanical complications may result from poorly designed RPDs due to neglecting the biomechanical principle which result from insufficient design information to the technician. Mechanical principles like support, retention and stability should be taken into consideration. Plaque accumulation and oral tissue damage should be minimized by the hygienic principles of the design[8-10]. An inadequate consideration to important clinical and biological factors can cause tissue damage. The final impression should be

made of a dimensionally stable elastomeric material by using a modified metal stock tray or a rigid special tray[11,12]. The responsibilities of the dental practitioners toward the dental laboratory technician and stated definite recommendations for dental educators to deal with the consequences in future[13].

**2. Aim of the study:**

To evaluate the knowledge and attitude of undergraduating students and interns in providing proper design of removable partial denture (RPD) to patients in dental schools of Benghazi \ Libya, to improve the undergraduate curriculum that can be beneficial for the newly graduating student and the practicing dentist. The null hypothesis was that there was no differnces between the knowledge and attitude of undergraduating students and interns in providing proper design of removable partial denture (RPD) to patients in dental schools of Benghazi \ Libya.

**3. Material and method:**

A cross-sectional study design was conducted among dental students and interns at the Faculties of Dentistry of both the University of Benghazi and LIMU. A convenience sampling method was employed. Ethical approval (no. 0220) was obtained from the Ethics Committee at the Faculty of Dentistry, University of Benghazi. An online-based questionnaire was used to collect data. The questionnaire included sixteen questions to assess knowledge and attitude about participants' understanding of constructing RPDs, and communication with dental laboratories. Data was collected over a period of 3 months (July -September 2024). Data was analyzed using SPSS (Ver.24), frequencies, and percentages were calculated for all categorical variables.

**4. Results:**

One hundred and thirty registered dentists completed the questionnaire. Table 1 presents RPD practices among participants. It was revealed that half (50%) of participants reported never providing RPD service, while 15.4% reported 1-2 cases per month. About a quarter (24.6%) of respondents base their decision for the treatment option of RPD on the number of natural teeth present, followed by 23.8% based on cost and patient desire. The majority (63.8%), indicated that they communicate with the laboratory by both marking on the primary cast and laboratory form. A smaller percentage, 8.5%, stated that they do not communicate with the laboratory during the RPD design process. Regarding the survey of the cast, less than half (40.8%) of respondents reported that they survey all the time, and more than one-third (35.4%) of respondents stated that they do sometimes, and 20.8% of respondents reported that they never survey the cast. Almost half (48.5%) reported that their dental technician follows their design instructions most of the time, followed by one quarter (25.4%) whose technician always follows their instructions. On the other hand, a small percentage 9.2%) reported that their technician never followed their design instructions.

**Table (1):** Respond to questions on RPD practices among participants.

Question	Respond	N (%)
----------	---------	-------

Q1. How often do you provide service of RPD to partially edentulous patient	Never	65 (50%)
	1-2 cases per month.	20 (15.4%)
	More than 3 cases per month	19 (14.6%)
	1-2 cases in 6 months	16 (12.3%)
	1-2 cases per year.	10 (7.7%)
Q2. On which basis do you decide on the treatment option of RPD	fixed not possible	24 (18.5%)
	number of natural teeth present	32 (24.6%)
	patient demand	20 (15.4%)
	excessive alveolar bone loss	20 (15.4%)
	cross stabilization	3 (2.3%)
	cost and patient desire	31 (23.8%)
Q3. While designing an RPD how do you communicate with the Laboratory	Verbally	13 (10%)
	Mark on the primary cast	10 (7.7%)
	On laboratory form	13 (10%)
	both b and c	83 (63.8%)
	None	11 (8.5%)
Q4. How often do you do survey	Never	27 (20.8%)
	No need	4 (3.1%)
	Sometimes	46 (35.4%)

	All the time	53 (40.8%)
Q5. Does your dental technician follow your design instruction	Never	12 (9.2%)
	Sometimes	22 (16.9%)
	Most of the time	63 (48.5%)
	Always	33 (25.4%)

Table (2) presents the participant attitudes regarding RPD design. A significant portion of participants (61.5%) believe that designing an RPD is the responsibility of the dentist, while 38.5% believe it's the responsibility of the dental technicians. The majority of respondents (57.7%) believe that surveying is the job of both a dental technician and a dentist.

**Table(2):** Responses to participant attitudes regarding RPD design.

Question	Respond	N (%)
Q6. In your opinion who should be responsible for designing an RPD	Dental laboratory technician	50 (38.5%)
	Dentist	80 (61.5%)
Q7. Is surveying the job of dental technician or a dentist	Dentist	23 (17.7%)
	Dental Technician	31 (23.8%)
	Both	75 (57.7%)
	Not required	1 (0.8%)

Table (3) presents the participant's knowledge regarding RPD design. It was found that less than one-third (30%) of participants were fully aware of how to transfer the need for tooth modification to the patient's mouth. The majority of respondents review their basic knowledge before starting an RPD design either most of the time (38.5%) or always (35.4%). 32.3% follow the ADA guidelines, which are considered a standard in the field, while one quarter (25.4%) rely on their notes and experiences in designing RPDs. 39.2% take rigidity into account when choosing a major connector, reporting that it is always a priority. 47.7% of respondents believe that indirect retainers are necessary in Kennedy's class I, II, and IV cases most of the time, while 21.5%, believe that indirect retainers are sometimes necessary.

Regarding the choices to modify the natural tooth structure, enameloplasty was the most preferred option, followed by changing the path of insertion and crowns, 40.8%, 20.8%, and 18.5% respectively. Only a small percentage of respondents 3.1% indicated that they would choose restoration as their preferred method for modifying the natural tooth structure. Gingivally approaching retainers were the most preferred choice among respondents, with 45.4%, followed by precession attachments, and occlusally approaching retainers, 24.6% and 19.2%, respectively.

**Table (3):** Responds to the understanding of RPD design and techniques.

Question	Respond	N (%)
Q8. Are you aware of how to transfer the need of tooth modification to be transferred in the patient's mouth	Not aware	13 (10%)
	Little bit	50 (38.5%)
	Aware	39 (30%)
	Fully aware	28 (21.5%)
Q9. When you start designing an RPD do you review your basic knowledge of designing	Never	3 (2.3%)
	Sometimes	31 (23.8%)
	Most of the times	50 (38.5%)
	Always	46 (35.4%)
Q10. Which reference do you follow in designing an RPD	BDJ	3 (2.3%)
	Mc Cracken's	16 (12.3%)
	Stewart's.	15 (11.5%)
	ADA guidelines	42 (32.3%)
	Other notes	33 (25.4%)
	No need	21 (16.2%)
Q11 . Are you aware of the function of dental implants in providing retention and support in RPD	Not aware	8 (6.2%)
	Little bit	33 (25.4%)
	Aware	58 (44.6%)
	Fully aware	31 (23.8%)
Q12 What do you think when selecting a major connector for RPD rigidity is an important factor	Never	6 (4.6%)
	Sometimes	29 (22.3%)
	Most of the time	44 (33.8%)
	Always	51 (39.2%)
	Never	5 (3.8%)

Q13. Do you agree when we design a clasp it should always be supported by a rest	Sometimes	44 (33.8%)
	Most of the time	37 (28.5%)
	Always	44 (33.8%)
Q14. Do we need to put indirect retainers in Kennedy's class I, II & IV cases	Sometimes	28 (21.5%)
	Most of the times	62 (47.7%)
	Always	40 (30.8%)
	Sometimes	28 (21.5%)
Q15. If you need to modify the natural tooth structure to create or reduce an undercut, what option will you prefer	Enameloplasty	53 (40.8%)
	Restoration	4 (3.1%)
	Crown	24 (18.5%)
	No need	8 (6.2%)
	Altering the RPD design	14 (10.8%)
	Change the path of insertion	27 (20.8%)
Q16. What type of retainer do you prefer in the maxillary esthetic zone for an RPD	Wrought Wire	14 (10.8%)
	Occlusally approaching	25 (19.2%)
	Gingivally approaching	59 (45.4%)
	Precession attachments	32 (24.6%)
	Wrought Wire	14 (10.8%)

### 5. Discussion:

A correct long-term prosthetic solution can be achieved with the patient's diagnosis of the remaining tissues. If an RPD is the chosen solution, analysis of support, followed by stability and only then, decide upon the necessary retentive elements are the systematic sequence. All other parts should be considered later[14]. The dentist may depend on the dental technician to design the partial denture due to weak undergraduate training in writing laboratory instructions which leads to inadequate communication between the dentist and technician[15]. Lynch and Allenref mentioned important guidelines for designing removable partial dentures. A faulty design of the prosthesis may result due to a lack of information on mechanical and biological principles for RPD design therefore, dental practitioners are responsible

legally and ethically that will not cause harm to oral structures[16,17]. The color coding may be used to mark the different components of RPD and similar terminology should be used by the dentist and the dental technician to get good communication. An online communication between dental clinics and dental laboratories may be provided by Computerized RPD systems[18]. It is not an acceptable practice to leave important parameters in removable prosthodontics like occlusal scheme, carving of posterior palatal seal, and information on finishing and contouring of the dental prosthesis to the decision of the dental technician due to insufficient education[16,17,19]. The interaction between dentists and dental technicians has been termed a “love-hate relationship” and the laboratory work authorization has been called the most frequently used and abused form of communication between them[20]. This study revealed the majority communicate with the laboratory by both marking on the primary cast and laboratory form. A smaller percentage do not communicate with the laboratory during the RPD design process. Less than half of respondents reported that they survey all the time, more than one-third of respondents stated that they do sometimes, and 20.8% of respondents reported that they never survey the cast. Almost half of the participants reported that their dental technician follows their design instructions most of the time, followed by one quarter whose technician always follows their instructions. On the other hand, a small percentage reported that their technician never followed their design instructions. In this study, a significant portion of participants believe that designing an RPD is the responsibility of the dentist, and the majority of respondents believe that surveying is the job of both a dental technician and a dentist. Preservation of existing oral structures is the primary purpose of treatment by removable partial denture and natural abutment teeth are selected to provide the necessary support, bracing, and retention for the removable prosthesis sometimes are unable to perform their task without some modification, therefore, altering the tooth's enamel surface or fabricating and placing a crown may be needed[21]. It was found that less than one-third of participants were fully aware of how to transfer the need for tooth modification to the patient's mouth and enameloplasty was the most preferred option and a small percentage of respondents would choose restoration as their preferred method for modifying the natural tooth structure. The Major connector of the cast partial denture should be rigid to resist flexing and torquing forces, it provides cross arch stability and resists displacement by functional stresses. An unequal distribution of forces may be caused by a flexible major connector which in turn may cause damage to the supporting structures[22]. The use of indirect retainers depends on any given case. It is important to apply an indirect retainer in Kennedy Class I, II and IV situations with long-span edentulous areas in the form of rests (occlusal, cingulum, incisal), Continuous bar or Cingulum bar[23]. In this survey 39.2% take rigidity into account when choosing a major connector, reporting that it is always a priority. 47.7% of

respondents believe that indirect retainers are necessary in Kennedy's class I, II, and IV cases most of the time, while 21.5%, believe that indirect retainers are sometimes necessary. A survey was made in commercial laboratories in Athens, Greece to record removable partial denture (RPD) retentive elements and abutment teeth in partially edentulous patients, Roach clasps were found to be used in the majority of cases whereas RPI clasps and attachments were rarely used[24]. Similarly, in our survey gingivally approaching retainers were the most preferred choice among respondents followed by precession attachments, and occlusally approaching retainers respectively.

## 6. Conclusion:

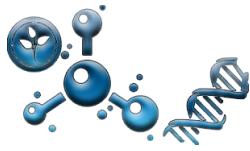
Within the limitation of this study we can conclude that; our undergraduated students have less chance to practice RPD that's why they miss some of the basic of treatment option for partial edentulism. On other hand, they belived in the communication with dental technicians . They aggreed that the survey and designing of RPD is mainly the responsibility of the dentist. Most of them considered ADA as a refrence. They belived in the importance of implant to support RPD , and the importance of major connector and gingivally approach retained in esthetic zone. Dental students in both universities (Benghazi and LIMU) showed acceptable level of knowledge about designing of RPD. Further practice is recommended.

## Refernces:

1. Nesreen Salim., et al. "First exposure of undergraduate students to removable prosthodontics concepts: opinions, attitudes and current trends in teaching". *Jordan Medical Journal* 55.3 (2021): 131-144.
2. Al-Angari N., et al. "Various classes of removable partial dentures: A study of prevalence among patients attending a dental and educational institute in Riyadh, Saudi Arabia". *The Saudi Dental Journal* 33.7 (2021): 656-660.
3. Sadig WM and Idowu AT. "Removable partial denture design: A study of a selected population in Saudi Arabia". *The Journal of Contemporary Dental Practice* 3.4 (2002): 40-53.
4. Khan MF., et al. "Knowledge and attitude regarding designing removable partial denture among interns and dentist; dental schools in Pakistan". *JPDA* 29.02 (2020).
5. Alshiddi IF. "Communication between dental office and dental laboratory: From paper-based to web-based". *Pakistan Oral and Dental Journal* 34.3 (2014).

6. Z. Afsharzand, B. Rashedi, V.C. Petropoulos: Communication between the dental laboratory technician and dentist: work authorization for fixed partial dentures. *J prosthodont*, 15 (2) (2006), pp. 123-128
7. American dental association: statement of prosthetic care and dental laboratories; 2000. p. 455.
8. Öwall B., et al. "Removable partial denture design: a need to focus on hygienic principles?" *International Journal of Prosthodontics* 15.4 (2020).
9. Phoenix RD., et al. "Stewart's clinical removable partial prosthodontics". Quintessence Chicago (2003).
10. Carr AB and Brown DT. "McCracken's Removable Partial Prosthodontics". 12th edition (2011): 95-128.
11. D. Lynch, P.F. Allen:Quality of written prescriptions and master impressions for fixed and removable prosthodontics: a comparative study.*Br Dent J*, 198 (1) (2005), pp. 17-20
12. C.D. Lynch, P.F. Allen:Quality of communication between dental practitioners and dental technicians for fixed prosthodontics in Ireland.*J Oral Rehab*, 32 (2005), pp. 901-905
13. C. Goodacre: Review of the literature predoctoral fixed prosthodontics education. *J Prosthet Dent*, 64 (3) (1990), pp. 319-325
14. N Samet , M Shohat: A systematic approach for removable partial denture design , *Refuat Hapeh Vehashinayim* 2003 Apr;20(2):71-6, 83.
15. Afsharzand Z, Rashedi B, Petropoulos VC. Communication between the dental laboratory technician and dentist: work authorization for fixed partial dentures. *J prosthodont* 2006;15(2):123–8.
16. Lynch D, Allen PF. Quality of written prescriptions and master impressions for fixed and removable prosthodontics: a comparative study. *Br Dent J* 2005;198(1):17–20.
17. Lynch CD, Allen PF. Quality of communication between dental practitioners and dental technicians for fixed prosthodontics in Ireland. *J Oral Rehab* 2005;32:901–5.

18. Davenport JC, Basker RM, Heath JR, Ralph JP, Glantz P-O, Hammond P. Communication between the dentist and the dental technician. *Br Dent J* 2000;189(9):471–4.
19. Tuominen R, Ranta K, Paunio L. Wearing removable partial dentures in relation to periodontal pockets. *J Oral Rehabil* 1989;16:119–26.
20. Leeper SH. Dentist and laboratory: a love-hate relationship. *Dent Clin North Am* 1979;23:87–99.
21. Wright WE. Abutment tooth modification for removable partial denture therapy. *Compendium*. 1989 Jan;10(1):40-3, 46-7. PMID: 2688890.
22. Bhojaraju N, Srilakshmi J, Vishwanath G. Study of deflections in maxillary major connectors: a finite element analysis. *J Indian Prosthodont Soc*. 2014 Mar;14(1):50-60. doi: 10.1007/s13191-012-0237-3. Epub 2012 Dec 27. PMID: 24604998; PMCID: PMC3935043.
23. Phoenix RD, Cagna DR, DeFreest, CF – editors. *Stewart's clinical removable partial prosthodontics*. 3th ed. Chicago: Quintessence Publishing Co.; 2003.
24. Polychronakis N, Sotiriou M, Zissis A. A Survey of Removable Partial Denture (RPD) Retentive Elements in Relation to the Type of Edentulism and Abutment Teeth Found in Commercial Laboratories, Athens, Greece. *Acta Stomatol Croat*. 2014 Sep;48(3):199-207. doi: 10.15644/asc48/3/4. PMID: 27688367; PMCID: PMC4872824.



Type of the Paper (Research Article)

## The use of golan gum in the targeted release of sulfasalazine to the large intestine based on pH sensitivity

Mahshid Sadeghi\*<sup>1</sup>

<sup>1</sup> Islamic Republic, Iran

**Citation:** Mahshid Sadeghi. The use of golan gum in the targeted release of sulfasalazine to the large intestine based on pH sensitivity. *Biomat. J.*, 3 (1), 14 – 32 (2024).

<https://doi.org/10.5281/znodo.5829408>

Received: 19 December 2024

Accepted: 24 December 2024

Published: 25 December 2024



**Copyright:** © 2023 by the authors. Submitted for possible open access publication under the terms and conditions of the Creative Commons Attribution (CC BY) license (<https://creativecommons.org/licenses/by/4.0/>).

\* Corresponding author e-mail: [Mahshid.sadeghi74@yahoo.com](mailto:Mahshid.sadeghi74@yahoo.com)

**Abstract:** Targeted drug delivery is one of the most important branches of pharmaceutical sciences, which is important for researchers in increasing the effectiveness of drugs and reducing drug toxicity by means of drug delivery carriers.

The formulation of drug delivery systems can increase the safety of the drug by reducing systemic side effects, preventing the release of the drug in the stomach and damaging it, and preventing the distribution of the drug in healthy tissues. It also prevents the decomposition of the drug and covers the bitter taste of the drug and reduces costs. The purpose of this research is to use the drug sulfasalazine to the colon in a drug delivery system based on azo hydrogels, which we cover with gellan polysaccharide, and to show its effect on the body's digestive system and the treatment of inflammatory bowel disease.

To do this, we first poured distilled water into the sample beaker and mixed it with a magnetic stirrer. Heating was done for one hour to completely dissolve gelatin. Then, the ground drug was added during the dissolution of gelatin. Stirring continued for three hours and after that we drained the samples in a plastic container and put them in the refrigerator. 30 ml of deionized water was added to 10 ml of each of the samples, then they were titrated separately using 10 M sodium hydroxide solution and 10 M hydrochloric acid. The dialysis bag was cut into several pieces, and then the bottom of the bag was closed with a piece of clean, suitable cotton soaked in PBS buffer, and 20 ml of samples were added to each bag. For each sample, 25 cc of isotonic PBS buffer with pH=0.7 was added to a 50 cc Falcon tube, and the dialysis bag and its contents were immersed in the Falcon tube. Then, optical absorption or ultraviolet light was read using a spectrophotometer in both environments inside the dialysis bag and outside the bag during different hours. Cytotoxicity test is done by several methods: NRU, CFU, MTT, XTT, in this research we used MTT test to check the toxicity of substances on cell life. We used the FTIR analysis test to identify unknown substances, determine the concentration and quality of the sample. This research, while confirming the slow release, showed that the maximum release of the drug is within 48 hours in the environment similar to physiological and isotonic conditions. The successful

development of nanoparticles for the oral method can change the treatment pattern of many diseases and have an important effect on the treatment results in the future.

**Keywords:** *golan gum, sulfasalazine, large intestine*

## 1. Introduction

Inflammatory bowel disease is a common disease in the digestive system that causes inflammation and ulceration in the inner wall of the large intestine and small intestine. This disease can be painful and sometimes debilitating and in some cases it can be life threatening. Inflammation can be limited to the intestinal wall or spread throughout the intestine, and finally it can cause another acute disease in different areas of the digestive system and anus.

Sulfasalazine is one of the main drugs. The most effective ones are for the treatment of inflammatory bowel disease. It is an anti-inflammatory drug that has two parts of 5-aminosalicyl, one acid and sulfapyridine, which are connected by an AZO bond, and it is taken orally. This drug is broken down in the acidic pH of the stomach and its pharmacological effect is lost. Drug release is a method in which by using the medical method and combining it with the engineering point of view, drugs or therapeutic molecules in general can be delivered more effectively to the desired target i.e. the treated area. Drug delivery to the colon is a new strategy that has received much attention. The selective release of drugs to the colon can not only control the required dose, but also reduce the systemic side effects caused by high doses. Peptide, protein, oligonucleotide drugs and vaccines can be good candidates for this route. Releasing the drug from the colon route and through the absorption of the cells of this route is another way of delivering drugs that are absorbed in small amounts from the previous parts of the digestive tract. However, there are some obstacles to choose this route for drug release. Different pH, long transit time from the mouth to the large intestine can be some of these obstacles that can be overcome by using pH-sensitive coatings. Polysaccharide di and azopolymeric coatings such as hyaluronic acid, galactomethane based systems and also azo hydrogels that can be destroyed by bacteria can be used to release the drug from the colon. Gellan polysaccharide iodine gum is biocompatible and non-cytotoxic, which is resistant to the acidic pH of the stomach, but is destroyed in the intestinal environment and causes the drug to be released at the target site. In this research, in order to deliver the drug sulfasalazine to the colon, we coated it with gellan iodide polysaccharide in a drug delivery system based on azo hydrogels.

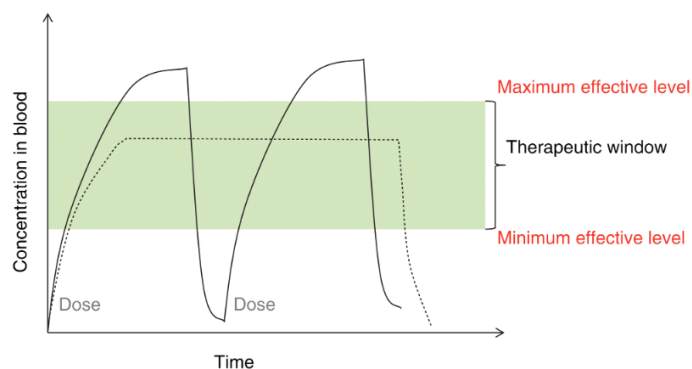


**Fig 1:** Showing the amount of drug concentration in blood with traditional drug delivery (dashed line) and controlled drug delivery (solid line)

Controlled drug release is a targeted control system that, by means of a biological stimulus, guarantees the release of a certain amount of drug at a certain time to achieve the desired therapeutic effect [2] despite the tremendous progress in this field in recent decades, the systems Drug delivery is not a new concept. The people of ancient China and Egypt, even before the word drug delivery, used this concept in the form of polymers and waxes with active medicinal agents. Since the industrial revolution in 1970, various technologies have been developed in the field of drug delivery [4 and 3].

The formulation of drug delivery systems can increase the safety of the drug by reducing systemic side effects, preventing the release of the drug in the stomach and damaging it, and preventing the distribution of the drug in healthy tissues. It also prevents the separation of a drug and also covers the bitter taste of the drug and reduces costs. All kinds of drugs, regardless of their molecular weight and solubility in water, can be loaded into biodegradable microparticles using different production techniques. In general, a targeted drug delivery system includes a drug, a carrier and a targeted ligand.

1) Target: In this system, it is the tissue, organ or cell that needs treatment.

2) Drug carrier: drug release is possible only from the drug site. Carriers, molecules or any system

There are others who are responsible for the successful transfer or transport of the drug to the target tissue.

Carriers are specially designed to hold the drug in their structure. This is possible by encapsulating the drug, or enclosing it.

## **Targeting mechanisms of the drug**

### **1: Physical targeting**

Physical targeting by various external forces such as: magnetic field [9], ultrasound [10], light [11], heat [12] and electric field [13] in order to accumulate or disperse the medicinal agent in the desired location. can be It seems that among these cases, the use of magnetic field, light and ultrasonic waves has found wider use, and among these, magnetic field has found wide commercial applications due to its cheapness and ease of use [16 14]. Drug delivery by ultrasound waves is another new method of drug delivery that combines ultrasound technology with microbubbles

containing medicinal compounds and facilitates cellular absorption by using an external ultrasound field. It is depicted schematically in the form of drug release to cancer tissue by sending ultrasound waves[17]

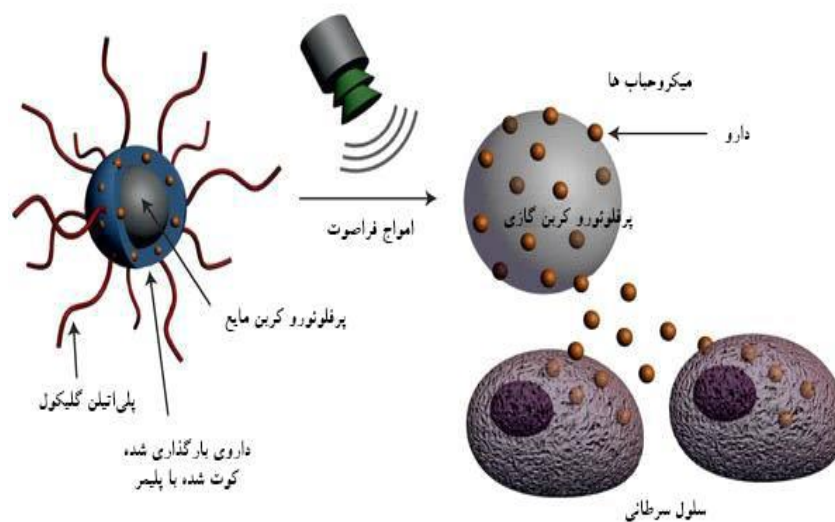


**Fig 2:** Sending ultrasound waves to microbubbles and drug release in cancer tissue

Controlled drug delivery systems have caused tremendous expansion and progress in the field of pharmaceuticals. In the pharmaceutical industry, one of the most vital needs is finding and making suitable drug carriers for drug delivery. As a result, the side effects of drugs are reduced due to the use of a small amount of drugs and effectiveness in certain areas. The drug delivery system without a target causes the distribution of the drug in the body and the effect of the drug on all areas of the body. This dispersion and distribution causes toxic effects on other areas as well as loss of important medicinal compounds. In medical engineering, the design of drug carriers for better diagnosis and treatment is very important in order to improve the management of diseases [23 22]. The presence of biological materials 1 is needed to design a stable and environmentally friendly drug carrier system, which can be natural polymers, metal compounds, synthetic and modified polymers. Compatibility with the environment and biodegradability of these materials have a significant effect on reducing toxic effects. A suitable drug carrier system has an effect on the absorption, distribution and rate of drug metabolism [24, 25]; This has been achieved by controlled drug delivery systems. Figure 3 shows the synthesis methods of different drug delivery systems.

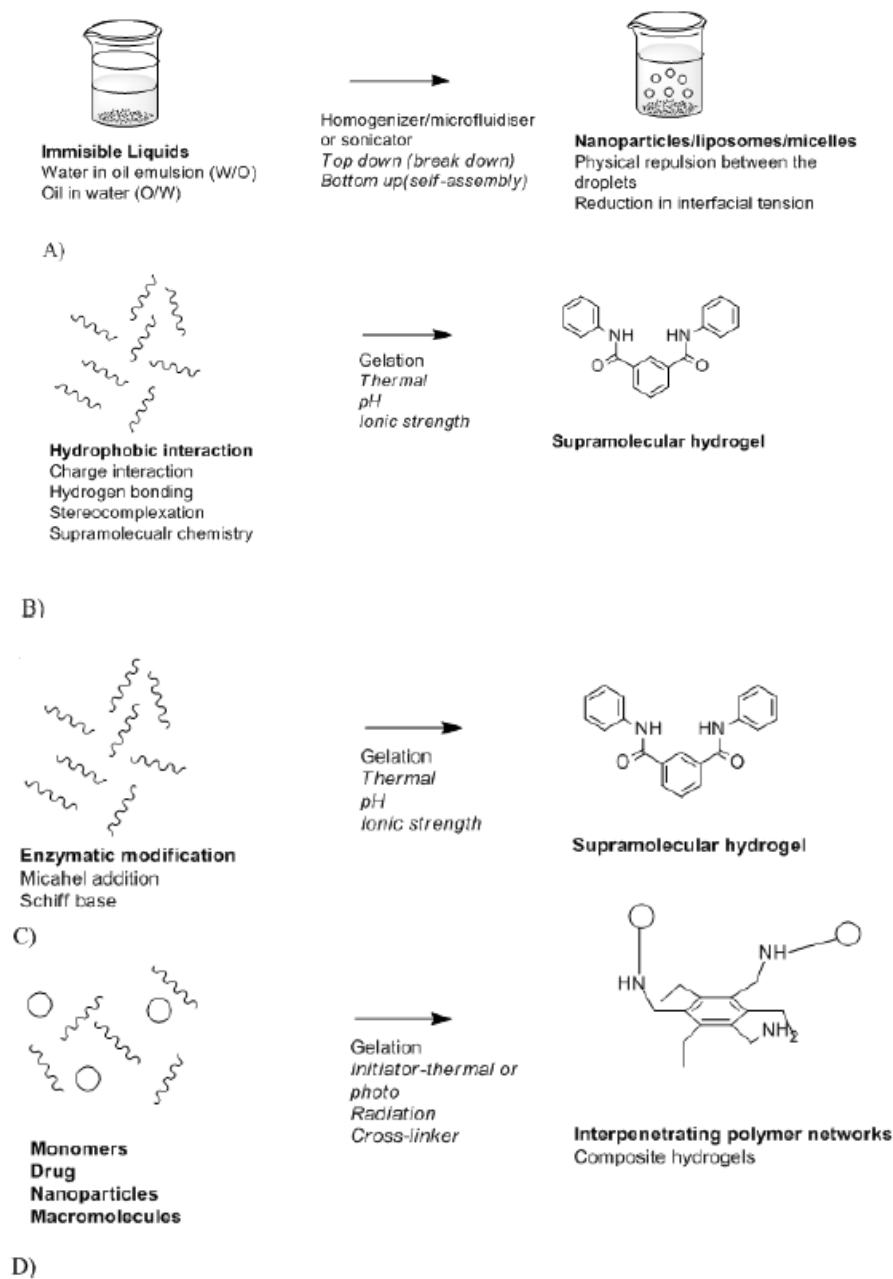


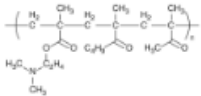
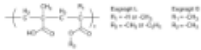
**Fig 3:** The different methods of synthesis of drug delivery systems.

### Drug release system based on polymer

In the drug release system, polymers (natural and synthetic) are used to improve the efficiency of this system. The most important factor for choosing a polymer is its biodegradability. Because when it enters the body, after the drug release process is completed, it is easily removed from the body. Also, the radical polymerization method is used for the synthesis of these macromolecules. Bioadhesion is defined as the adhesion between the polymer and the biological structure. The existence of polymers is essential to create this state of adhesion [27]. In recent years, a number of

bioadhesive polymers have been considered very important in the drug release system: poly(acrylic acid), carboxymethyl acid. Cellulose and hydroxypropyl methyl cellulose. Among these polymers, polyacrylic acid 1 (especially in the cross-linked state) is a very good option, due to its nature. Hydrophilicity, negative charge and high flexibility are selected.

**Common pH-sensitive polymers used in drug delivery.**

Name	Chemical structure	Clinical indication	Refs.
Aminoalkyl methacrylate copolymer (Eudragit E)		Taste-masking	[28-32]
Poly(methacrylic acid-co-methyl methacrylate) (Eudragit L/S)		Protection of acid-degradable drugs, colon delivery	[6,35-43]
Hydroxypropyl-methylcellulose phthalate (HPMC-P)		Protection of acid-degradable drugs, colon delivery	[6]

**gellan gum :**



**Fig 4:** Gellan gum preparation.

This gum is an anionic polymer made of beta-diglucose, beta-diglucuronic acid and alpha-l-rhamnose units in a ratio of 1:1:2.

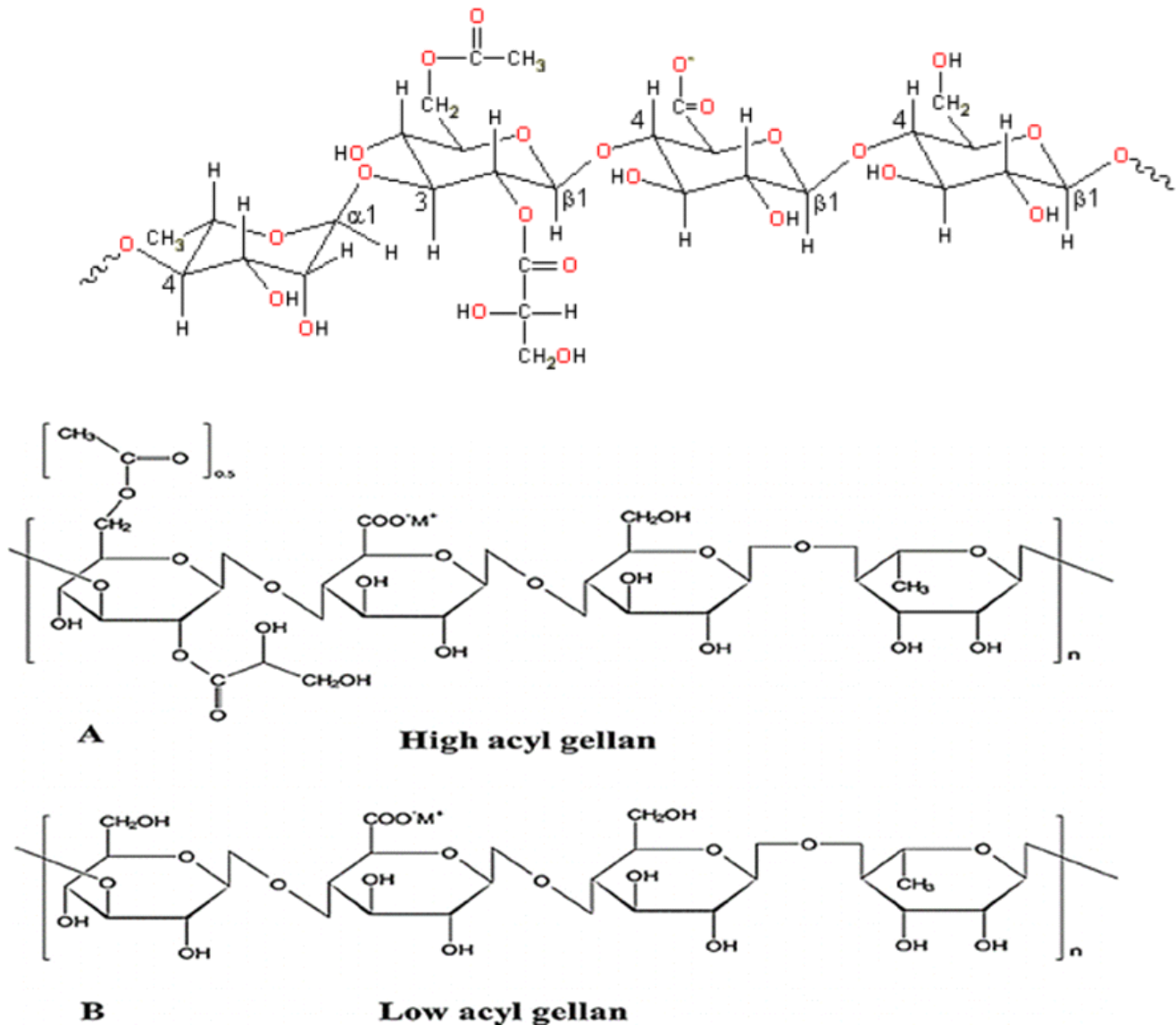
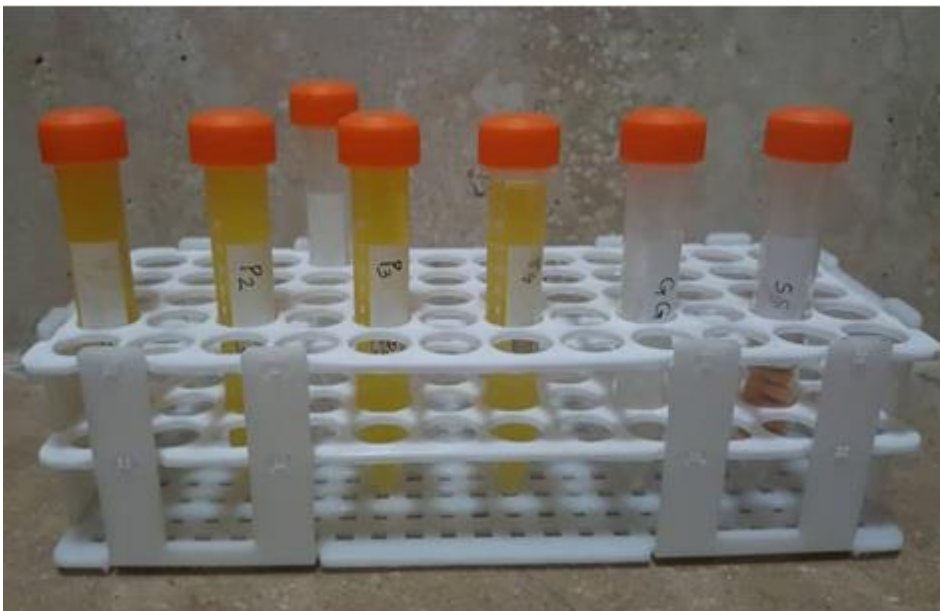


Fig 5: Chemical structure of gellan.

## 2. Material and method:

The gelatin sample was poured into a beaker and distilled water was added to it (Table 2). Then the beaker was covered and mixed by a magnetic stirrer. It was heated to a temperature of 90 degrees Celsius for one hour until dissolution. It is worth mentioning that 90 degrees Celsius is the temperature required to dissolve gelatin gum. After one hour, the ground drug was added to it while dissolving gelatin. Then for 3 hours it was stirred by a magnetic stirrer. The prepared samples were emptied into plastic containers and kept in the refrigerator.



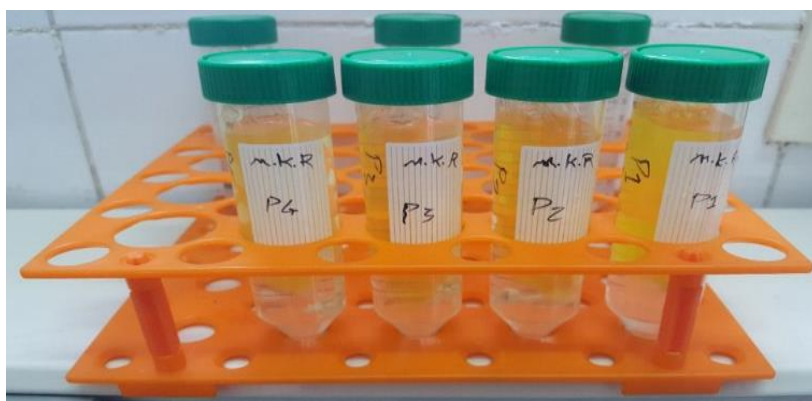
30 ml of deionized water was added to 10 ml of each of the samples, then they were titrated separately using 0.1 M hydrochloric acid solution and 0.1 M sodium hydroxide. It is in milliliters of acid or base consumed until the target pH is reached. A pH meter was used to measure the final pH of the samples



The pouch was cut into 17 cm pieces. Then the bottom of the bag with a piece of thread fits perfectly Cleaned and quenched with PBS buffer. 20 ml of samples were added to each dialysis bag.



For each sample, 25 cc of isotonic PBS buffer with pH = 7 was added to a 50 cc Falcon tube, and the dialysis bag with its contents was immersed in the Falcon tube.



Then absorb O.D. Absorbance (or UV light at a wavelength of 359 nm (359 nm  $\lambda$ ) was read using a spectrophotometer in both environments inside the dialysis bag and outside the bag during 1, 2, 4, 8, 24 and 48 hours.

### Cytotoxicity test

Cell experiments were performed at the Institute Pasteur center in the north of the country (AML) and in the cell culture laboratory. Fibroblast cells were obtained from the cell bank of the Institut Pasteur of Iran and were cultured in DMEM culture medium containing 10% FBS and 1% antibiotics penicillin and streptomycin (relative to 1 to 1) were cultured. Then the cells that have grown were separated from the culture medium with trypsin and centrifuged at 1500 rpm for 10 minutes at 4 degrees Celsius. Then 200 microliters of the cell suspension in the number of 5000 Cells were cultured in BIOFIL 96-well microplates for 24 hours (Figure 3 10) (Figure 3 11) (Figure 3 12). Next, each sample was mixed with the culture medium in the order of Table (3 4) and in each The well was added.

The microplates were placed in an incubator for 24, 48, and 72 hours at 37°C, 95% humidity, and 5% 2CO concentration (Figure 13). After 24, 48, and 72 hours, the effect Each sample on the mentioned cell line was checked by MTT colorimetric test method. The cytotoxicity test is performed according to the ISO10993-5 standard and with three methods: NRU test, CFU test, MTT test, and XTT test. The most common method in evaluating cytotoxicity is the cell survival assay using the MTT or (3-4,5-dimethylthiazol-2-yl-2,5-diphenyltetrazolium bromide) method.

### 3. Results and Discussion:

Diagram (4-7) compares the four Fourier transform infrared spectroscopic spectra of the four produced hydrogels in reverse Y-axis. In the area surrounded by the red circle, it can be seen that the spectra are in complete agreement and only in the amount The transmission spectrum clearly shows a change in the range of 1-Cm 2000 500. This difference in the transmission spectrum is visible in all parts of the spectrum, but it is more clear in this range.

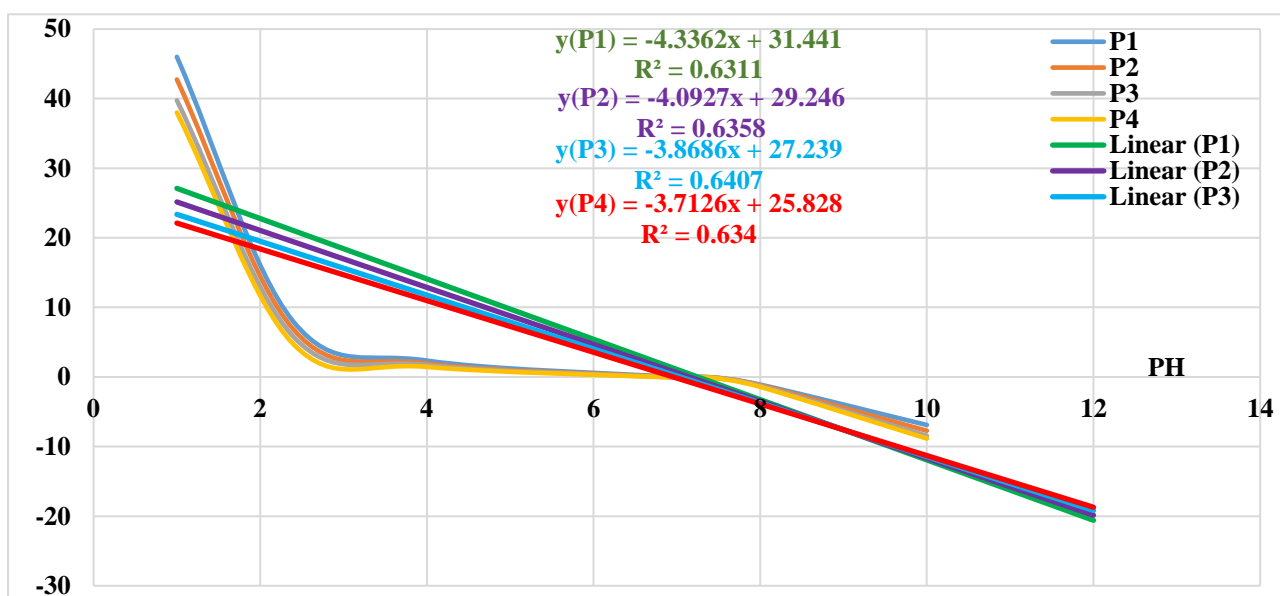
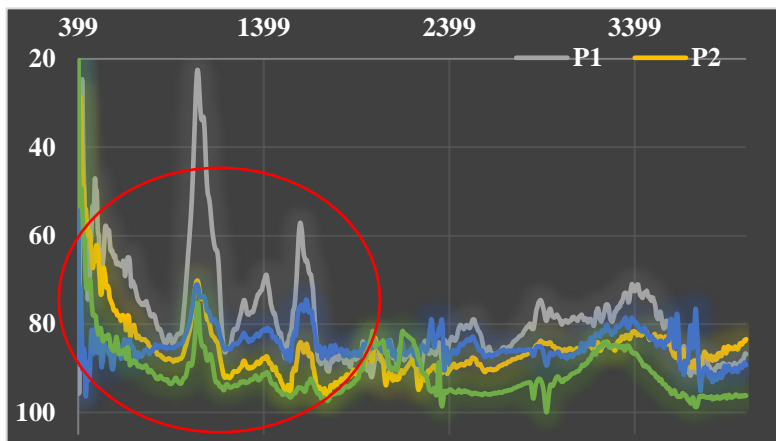


Diagram number (4-10) shows the drug release in standard conditions and in the presence of the semi-permeable barrier of the dialysis bag with a cut-off of 14 kilodaltons over time in a linear fashion. The amount of GG is far away from the product P4, which has the lowest amount of GG, and this indicates that GG is effective in releasing the drug more slowly. Also, in the first 4 hours of the study, all four products showed almost the same behavior, but in the eighth hour and later The difference between different products has become significant.

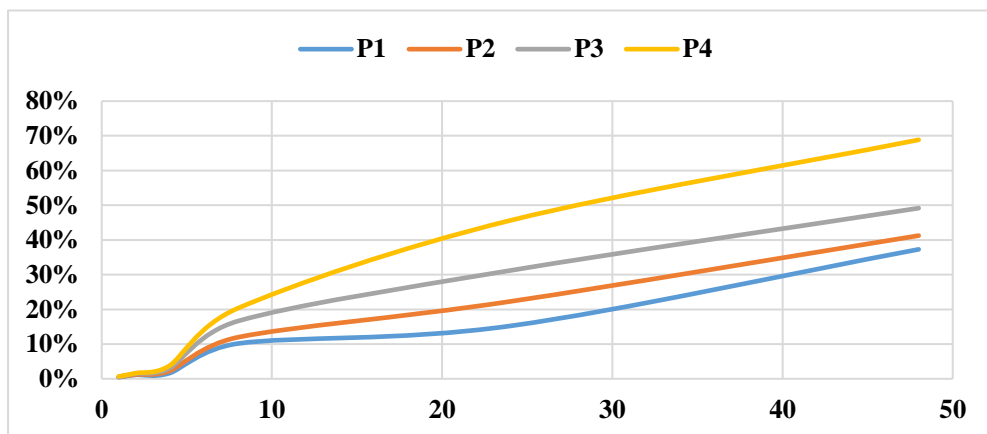


Diagram (4-10): Linear diagram of sulfasalazine drug release in four products P1, P2, P3 and P4 separately for each product

### Cytotoxicity

In order to check the level of cytotoxicity of the product and the components used to make the product, normal human fibroblast cells were treated using the prepared products and sulfasalazine and gellan gum. After a period of 24, 48 and 72 hours from the proximity of cells with separate medicinal compounds and products; It was investigated using the MTT Assay method. The results of the light absorption obtained by the ELISA device along with the analysis of the results are given in tables (3-4), (4-4) and (4-5).

Conc. (µg/ml)	OD1	OD2	OD3	Viability 1	Viability 2	Viability 3	Average	SD	SEM	Cell Inhibition	Ttest
P1	0.377	0.362	0.347	84.80	80.16	75.00	79.99	4.90	2.83	20.01	0.019419
P2	0.389	0.363	0.375	88.00	80.42	82.29	83.57	3.95	2.28	16.43	0.018705
P3	0.378	0.392	0.381	85.07	88.10	83.85	85.67	2.18	1.26	20.45	0.007659
P4	0.394	0.383	0.387	89.33	85.71	85.42	86.82	2.18	1.26	13.18	0.009002
G1	0.407	0.412	0.436	92.80	93.39	98.18	94.79	2.95	1.70	5.21	0.092232
G3	0.429	0.443	0.435	98.67	101.59	97.92	99.39	1.94	1.12	0.61	0.640628
SS	0.401	0.345	0.364	91.20	75.66	79.43	82.10	8.11	4.68	17.90	0.062036
Control	0.434	0.437	0.443	100.00	100.00	100.00	100.00	0.00	0.00	0.00	
Blank			0.059								

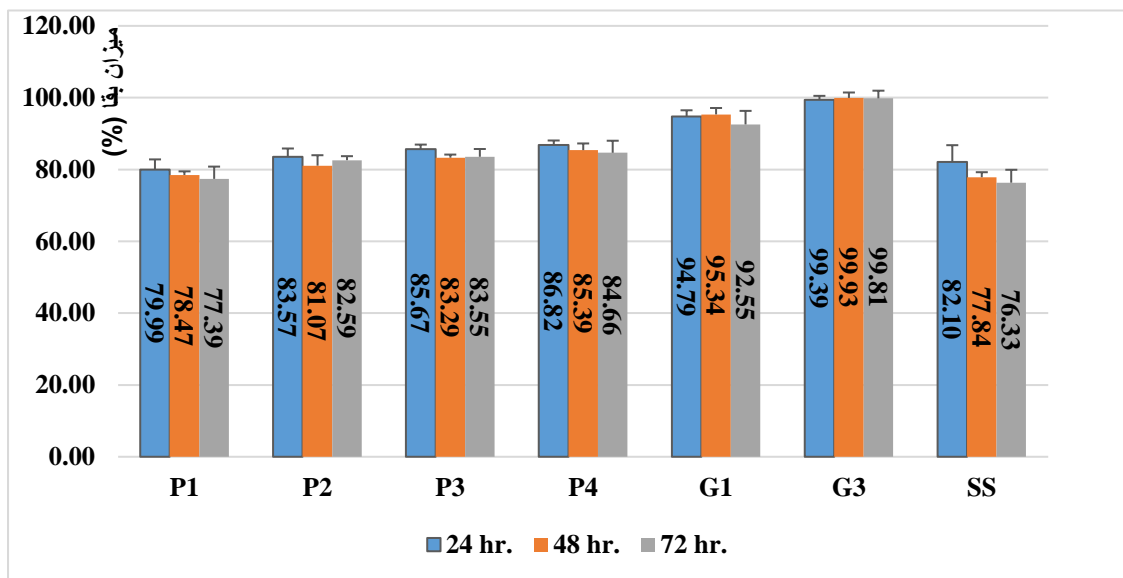
Absorption, average survival rate and inhibition of different samples and relevant statistical indicators within 24 hours of placement of human fibroblast cells in the vicinity of different samples

Conc. (µg/ml)	OD1	OD2	OD3	Viability 1	Viability 2	Viability 3	Average	SD	SEM	Cell Inhibition	Ttest
P1	0.462	0.479	0.481	76.52	79.99	78.89	78.47	1.77	1.02	21.53	0.002246
P2	0.517	0.464	0.483	86.77	77.18	79.25	81.07	5.05	2.91	18.93	0.022865
P3	0.489	0.502	0.509	81.55	84.29	84.03	83.29	1.51	0.87	16.71	0.002710
P4	0.528	0.492	0.514	88.82	82.42	84.94	85.39	3.22	1.86	14.61	0.015857
G1	0.564	0.544	0.587	95.53	92.14	98.35	95.34	3.11	1.79	4.66	0.121634
G3	0.601	0.571	0.597	102.42	97.19	100.18	99.93	2.62	1.51	0.07	0.968959
SS	0.454	0.475	0.483	75.03	79.24	79.25	77.84	2.43	1.41	22.16	0.003997
Control	0.588	0.586	0.596	100.00	100.00	100.00	100.00	0.00	0.00	0.00	
Blank			0.051								

Absorption, average survival rate and inhibition of different samples and relevant statistical indicators during 48 hours of placement of human fibroblast cells in the vicinity of different samples

Conc. (µg/ml)	OD1	OD2	OD3	Viability 1	Viability 2	Viability 3	Average	SD	SEM	Cell Inhibition	Ttest
P1	0.507	0.483	0.462	82.58	78.65	70.93	77.39	5.92	3.42	22.61	0.022115
P2	0.519	0.496	0.526	84.75	81.02	82.01	82.59	1.93	1.12	17.41	0.004093
P3	0.511	0.531	0.514	83.30	87.41	79.93	83.55	3.74	2.16	20.45	0.016836
P4	0.547	0.522	0.505	89.84	85.77	78.37	84.66	5.81	3.36	15.34	0.044650
G1	0.572	0.589	0.545	94.37	97.99	85.29	92.55	6.54	3.78	7.45	0.187439
G3	0.594	0.622	0.613	98.37	104.01	97.06	99.81	3.70	2.13	0.19	0.938277
SS	0.497	0.485	0.452	80.76	79.01	69.20	76.33	6.23	3.60	23.67	0.022317
Control	0.603	0.6	0.63	100.00	100.00	100.00	100.00	0.00	0.00	0.00	
Blank			0.052								

Absorption, average survival rate and inhibition of different samples and relevant statistical indicators during 72 hours of placement of human fibroblast cells in the vicinity of different samples



#### 4. Conclusion:

Many new drugs are only used by injection. Alternative methods of injection, to Especially the oral method, compared to the injection method, is very desirable because it is more convenient and seeks the patient's satisfaction. Although the oral method has many challenges due to the presence of barriers in the digestive system, polymeric nanoparticles can be used to overcome the pH and enzyme barriers, but the barriers of intestinal permeability It remains an important challenge. So far, many methods have been used to overcome the intestinal epithelial barrier to effectively deliver biological drugs and nanomedicines. The tests performed in an artificial environment to check the release of salt from hydrocolloids seem reliable, acceptable and repeatable and can be compared with different structures of gels and other materials in the future. Adhesive mucilaginous materials prolong the stay time in the intestine by using the mucous layer of the intestines and increase the concentration of drugs near the surface of the epithelial cells. In addition, there are many penetration-enhancing mucosal adhesions that open tight junctions between epithelial cells so that drugs and pharmaceutical agents can pass through this barrier. Other methods on targeting routes Natural transcytosis is focused on including the M cell, the vitamin B12 pathway, and the FcRn pathway. Recent studies have shown that targeting transcytosis pathways can effectively deliver drugs and nanomedicines orally, but more research is needed before these technologies can be used clinically. Oral drug delivery system is being developed for many different applications, such as oral drug delivery of chemotherapeutic agents for cancer treatment, local drug delivery to the intestine for the treatment of inflammatory bowel disease, and mucosal oral vaccination. Many proteins, especially insulin for the treatment

of diabetes, have been loaded into nanoparticles for oral use. The successful development of nanoparticles for the oral method can change the treatment pattern of many diseases and have an important effect on the treatment results in the future. This research, while confirming the slow release, showed that the maximum drug release within 48 hours is similar to physiological conditions and isotonic conditions.

## References:

- [1] Vermonden T, Censi R, Hennink WE. Hydrogels for protein delivery. *Chem Rev.* 2012; 112(5):2853–88. [PubMed: 22360637].
- [2] Goonoo N., Bhaw-Luximon A., and Jhurry D., Drug Loading and Release from Electrospun Biodegradable Nanofibers, *J. Biomed. Nanotech.*, 10, 2173-2199, 2014.
- [3] Reddy P.D. and Swarnalatha D., Recent Advances in Novel Drug Delivery Systems, *Int. J. Pharm. Tech. Res.*, 2, 2025-2027, 2010.
- [4] Mainardes R.M. and Silva L.P., Drug Delivery Systems: Past, Present, and Future, *Curr. Drug Targets.*, 5, 449-455, 2004.
- [5] Nikander K., Drug Delivery Systems, *J. Aerosol. Med.*, 7, 19-24, 1994.
- [6] Strebhardt, K. and A. Ullrich, Paul Ehrlich's magic bullet concept: 100 years of progress. *Nature Reviews Cancer*, 2008, 8(6): p. 473-480.
- [7] Torchilin, V.P., Drug targeting. *European Journal of Pharmaceutical Sciences*, 2000, 11: p. S81-S91.
- [8] Lübke, A.S., C. Alexiou, and C. Bergemann, Clinical applications of magnetic drug targeting. *Journal of Surgical Research*, 2001, 95(2): p. 200-206.
- [9] Rapoport, N., D. Christensen, H. Fain, L. Barrows, and Z. Gao, Ultrasound-triggered drug targeting of tumors in vitro and in vivo. *Ultrasonics*, 2004, 42(1): p. 943-950.

- [10] Lin, H.-M., W.-K. Wang, P.-A. Hsiung, and S.-G. Shyu, Light-sensitive intelligent drug delivery systems of coumarin-modified mesoporous bioactive glass. *Acta biomaterialia*, 2010, 6(8): p. 325-365.
- [11] Meyer, D.E., B. Shin, G. Kong, M. Dewhirst, and A. Chilkoti, Drug targeting using thermally responsive polymers and local hyperthermia. *Journal of controlled release*, 2001, 74(1): p. 213-224.
- [12] Langer, R., Drug delivery and targeting. *Nature*, 1998, 392(6679): p. 5-10.
- [13] Widder, K.J., A.E. Senyei, and D.G. Scarpelli, Magnetic microspheres: a model system for site specific drug delivery in vivo. *Experimental Biology and Medicine*, 1978, 158(2): p. 141-146.
- [14] Chong Li., Wang J., Y.Wang Y., Recent Progress in Drug Delivery , *Acta Pharmaceutica Sinica B*, 9, 1145-1162, 2019.
- [15] Klibanov, A.L., Microbubble contrast agents: targeted ultrasound imaging and ultrasound-assisted drug-delivery applications. *Investigative radiology*, 2013, 48(3): p. 354-362.
- [16] Ngoepe M., Choonara Y.E., Integration of Biosensors and Drug Delivery Technologies for Early Detection and Chronic Management of Illness, *Journal Sensors*, 13, 7680-7780, 2013.
- [17] Hirsjarvi, S., C. Passirani, and J.-P. Benoit, Passive and active tumour targeting with nanocarriers. *Current drug discovery technologies*, 2011, 8(3): p. 188-196.
- [18] Gu, F.X., et al., Targeted nanoparticles for cancer therapy. *Nano today*, 2007, 2(3): p. 14-21.
- [19] Ghasemzadeh H., Rashvand H., Sodium Alginate/Talc-g-Poly Sodium Acrylate Nanocomposite for Delivery of Indomethacin, *International Seminar on Polymer Science and Technology*, 2014.
- [20] Lin Y. S., Tsai C. P., Huang H.Y., Kuo C. T., Hung Y., Huang D. M., Chen Y. C., Mou C.Y. Well-ordered mesoporous Silica Nanoparticles as Cell Markers, *Journal of Chemistry Materials*, 17, 4570-4573, 2005.
- [21] Sijja, H.K.; East, M.P.; Mao, H.; Wang, Y.H.; Nie, S.; Yang, L. Development of multifunctional nanoparticles for targeted drug delivery invasive imaging of therapeutic effect. *Curr. Drug Discov. Technol.* 2009, 6, 43–51.

- [22] Theodorescu D., Wittke S., Ross M.M., Walden M., Conaway M., Mischak H., Frierson H., Discovery and Validation of New Protein Biomarkers for Urothelial Cancer: A Prospective Analysis, *The Lancet Oncology*, 7, 230–240, 2006.
- [23] Deo, S.P.; Moschou, E.A.; Peteu, S.F.; Bachas, L.G.; Daunert, S. Responsive drug delivery system. *Anal. Chem.* 2003, 75, 207-213.
- [24] Emerich D.F., Thanos C.G., The Pinpoint Promise of Nanoparticle Based Drug Delivery and Molecular Diagnosis, *Biomolecular Engineering*, 23, 171–184, 2006.
- [25] Kudela P., Koller, V.J., Lubitz. Bacterial Ghost (BGs)-advanced Antigen and Drug Delivery System, *Vaccine*, 28, 5760–5767, 2010.
- [26] Omidi S., Pirhayati M., Kakanejadifard A., Co-delivery of Doxorubicin and Curcumin by a pH Sensitive, Injectable, and in Situ Hydrogel Composed of Chitosan, Graphene and Cellulose Nanowhisker, *Carbohydrate Polymers*, 231, 115745, 2019.
- [27] Banihashem S., Nezhati M.N., Panahia H.A., Synthesis of Chitosan-grafted-Poly(N vinylcaprolactam) Coated on the Thiolated Gold Nanoparticles Surface for Controlled Release of Cisplatin, *Carbohydrate Polymers*, 227, 115333, 2019.
- [28] Wichterle O. and Lim D., “Hydrophilic Gels in Biologic Use,” *Nature*, 185,117-118, 1960.
- [29] Nagam S.P., Jyothei A.N., Poojitha J., Aruna S., and Nadendla R.R., “A Comprehensive Review on Hydrogels,” *Int. J. Curr. Pharm. Res.*, 8, 19-23, 2016.
- [30] Morkhande V.K., Pentewar R.S., Gapat S.V., Sayyad S.R., Amol B.D., Sachin B., and Sandip K., “A Review on Hydrogel,” *Indo Am. J. Pharm. Res.*,6, 4678-4689, 2016.
- [31] Laftah W.A., Hashim S., and Ibrahim A.N., “Polymer Hydrogels: A Review,” *Polym. Plast. Technol. Eng.*, 50, 1475-1486, 2011.
- [32] Ullah F., Bisyrul M., Othman H., Javed F., Ahmad Z., and Akil H.M., “Classification, Processing and Application of Hydrogels: A Review,” *Mater. Sci. Eng., Part C*, 57, 414-433, 2015.

- [33] Phillips GO, Williams PA. Handbook of hydrocolloids. New York: CRC Press; 2000.
- [34] Jampen S, Britt IJ, Tung MA. Gellan polymer solution properties: dilute and concentrated regimes. Food Res Int 2000; 3: 579-86.
- [35] Martínez-Padilla LP, López-Araiza F, Tecante A. Steady and oscillatory shear behavior of fluid gels formed by binary mixtures of xanthan and gellan . Food Hydrocolloids 2004; 18: 471-81.
- [36] Vaidya A, Jain S, Agrawal RK, Jain SK. Pectin-metronidazole prodrug bearing microspheres for colon targeting. J Saudi Chem Soc 2015;19:257-64.
- [37] Peppas NA, Wood KM, Blanchette JO. Hydrogels for oral delivery of therapeutic proteins. Expert Opin Biol Ther. 2004; 4(6):1–7. [PubMed: 14680464].
- [38] Malekzade R, Varshosaz J, Merat S, Hadidchi S, Mirmajlesi SH, Vahedi H, et al. Crohn's, Disease: a review of 140 cases from Iran. Irn J Med Sci 2000; 25: 138-43.
- [39] Ebrahimi Daryani N, Mohammadi HR, Ayermalou M. Clinical and epidemiological characteristics in ulcerative colitis patients referred to Imam Hospital 1995-2000. Tehran University Medical Journal (TUMJ) 2001; 59: 80-5.
- [40] Aghazadeh R, Zali MR, Bahari A, Amin K, Ghahghaie F, Firouzi F. Inflammatory bowel disease in Iran: A review of 457 cases. J Gastroenterol Hepatol 2005; 20: 1691-5.
- [41] Masjedi Zadeh R, Hajiani E, Hashemi SJ, Azmi M, Shayesteh AK. Epidemiological features of inflammatory bowel disease in Khozestan. Scientific Medical Journal 2007; 6: 54-63.
- [42] Kornbluth, A, Sachar, DB. Ulcerative colitis practice guidelines in adults (update): American College of Gastroenterology, Practice Parameters Committee. Am J Gastroenterol 2004; 99:1371.
- [43] Friedman S, Blumberg RS. Inflammatory Bowel disease. In: Kasper DL, Fauci AS, Longo DL, et al. Harrison's Principles of Internal Medicine. 16th edition. New York:McGrawhill; 2005:1776- 1789.
- [44] Sutherland L, Roth D, Beck Y, et al. Oral 5- aminosalicylic acid for inducing remission in ulcerative colitis. Cochrane Database Syst Rev 2000; CD000543.

[45] Schroeder KW, Tremaine WJ, Ilstrup DM. Coated oral 5-ASA therapy for mildly to moderately acute ulcerative colitis. *New Engl. J Med* 1987; 317(26): 1625-1629.

[46] Linn FV, Peppercon MA. Drug therapy for inflammatory bowel disease *AM J Surg* 1992; 164: 85-89.

[47] Meyer S. The place of oral 5-ASA in the therapy of ulcerative colitis. *AM J Gastroenterol* 1988; 83(1): 64-66.

[48] Harish NM, Prabhu P, Charyulu RN, Gulzar MA, Subrahmanyam EV. Formulation and Evaluation of in situ Gels Containing Clotrimazole for Oral Candidiasis. *Indian J Pharm Sci* 2009; 71(4): 421-427



Type of the Paper (Research Article)

## AMORPHOUS ALLOYS: A STUDY ON THEIR APPLICATIONS AS BIOMATERIALS

NASCIMENTO. <sup>1,\*</sup>, COSTA, A. C. F. M. <sup>2</sup>

<sup>1,2</sup> Laboratory of Ceramic Materials Synthesis, Federal University of Campina Grande, 882 Aprígio Veloso Street—Bodocongó, Campina Grande 58429-900, PB, Brazil

**Citation:** NASCIMENTO, COSTA, A. C. F. M. AMORPHOUS ALLOYS: A STUDY ON THEIR APPLICATIONS AS BIOMATERIALS. *Biomat. J.*, 3 (1), 33 – 53 (2024).

<https://doi.org/10.5281/znodo.5829408>

Received: 11 November 2024

Accepted: 24 December 2024

Published: 25 December 2024

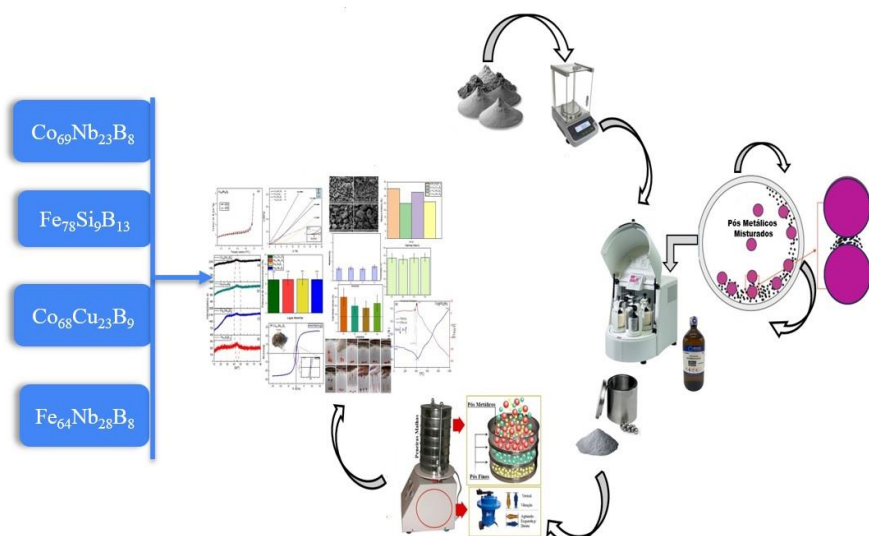


**Copyright:** © 2023 by the authors. Submitted for possible open access publication under the terms and conditions of the Creative Commons Attribution (CC BY) license (<https://creativecommons.org/licenses/by/4.0/>).

\* Corresponding author e-mail: [luciano.nascimento@estudante.ufcg.edu.br](mailto:luciano.nascimento@estudante.ufcg.edu.br)

**Abstract:** In this work, the amorphous alloys Co<sub>69</sub>Nb<sub>23</sub>B<sub>8</sub>, Fe<sub>78</sub>Si<sub>9</sub>B<sub>13</sub>, Co<sub>68</sub>Cu<sub>23</sub>B<sub>9</sub> and Fe<sub>64</sub>Nb<sub>28</sub>B<sub>8</sub> were synthesized by high energy milling (HEM) and investigated as promising biomaterials for bone tissue regeneration. The amorphous alloys Co<sub>69</sub>Nb<sub>23</sub>B<sub>8</sub>, Fe<sub>78</sub>Si<sub>9</sub>B<sub>13</sub>, Co<sub>68</sub>Cu<sub>23</sub>B<sub>9</sub> and Fe<sub>64</sub>Nb<sub>28</sub>B<sub>8</sub>, were milled using a load of 20 g, with a ball-to-powder weight ratio of 20:1, rotation speed 300 rpm, grinding time was 15 h, and used ethyl alcohol (C<sub>2</sub>H<sub>6</sub>O) as a process controlling agent (PCA) as a grinding medium and an argon atmosphere. The amorphous alloys were subjected to characterization by XRD, FTIR, textural analysis, SEM, thermogravimetric analysis (TGA-DTA), magnetic measurements (VSM), mechanical tests and in vitro cytotoxicity tests. Finally, it was observed through the cytotoxic profile that the safe concentration, at which cell viability was greater than 70%, had promising potential for applicability as a metallic biomaterial for bone tissue regeneration and temporary implants in orthopedics.

**Keywords:** Amorphous Alloys; Biomedical Applications; Bone Tissue Regeneration; High Energy Milling (HEM).



Graphical Abstract

## 1. Introduction

Increased life expectancy has led to a rapid aging of the population and, consequently, a higher incidence of bone diseases, such as osteoporosis, as well as bone fractures [1,2]. However, the search for an ideal biomaterial still persists as one of the greatest challenges in the medical field, such as its application for bone tissue regeneration and implants [3]. There are many clinical reasons for the development of new materials to replace human bone, such as in the reconstruction of defects, including the need for orthopedic implants that are resistant to corrosion and mechanically more suited to their biological environment [4,5].

Bone is a mature connective tissue that provides functionality for our bodies, protection of vital organs, and a stable base for muscle and joint function. Bone also plays an important physiological role in supporting hematopoietic and mineral homeostasis activities in our bodies, being the main protective barrier for vital organs [6]. Current surgical procedures for bone repair include transplantation of tissue grafts of natural origin or biomaterials developed from various methods, such as powder metallurgy and rapid solidification [7].

The most common reconstructive graft is autograft, which involves harvesting the patient's tissue from a donor site and transplanting it to the damaged or deficient recipient site [8]. There are some limitations to these techniques, as autografts have limited availability and can result in trauma and invasive (surgical) procedures in patients [9]. These graft limitations have led to the development and use of biomaterials as substitutes for the bone tissue regeneration process [10].

The purpose of the biomaterial is to play a fundamental role in bone tissue regeneration by temporarily acting as a support structure that allows the gradual distribution of stress in affected areas, thus providing a pathway for cell growth until the bone tissue is fully recovered [11]. In order to achieve this purpose, the structure must maintain its shape and adequate mechanical characteristics throughout the regeneration process, until the injured region is completely recovered [12,13].

As a metallic biomaterial, amorphous alloys were first synthesized in 1960 by Pol Duwez using the rapid cooling technique (on the order of  $10^5 - 10^6 \text{ K s}^{-1}$ ) in a binary metal alloy system  $\text{Au}_{80}\text{Si}_{20}$ , and attracted the attention of researchers around the world due to their special properties [14,15]. Amorphous alloys have a long-range disordered atomic structure and exhibit unique magnetic properties, high mechanical strength, low elastic modulus, good corrosion resistance, and satisfactory biocompatibility for biomedical applications [16].

Due to the importance of amorphous alloys, several technologies have been developed to obtain them over time, among which are the chilling of molten metal into ribbon forms (melt-spinning) [17], arc furnace casting (cooled metal mold) [18], centrifugal casting [19], gas atomization (hot or cold extrusion) [20], spray forming [21], chemical reduction [22], electrodeposition [23] and high energy milling (HEM) [24]. Among the methods mentioned, HEM stands out for being a powder processing technique that allows the production of homogeneous materials from the mixture of elementary powders [25]. Thus, the objective of the present work was the synthesis of amorphous alloys with the compositions  $\text{Co}_{69}\text{Nb}_{23}\text{B}_8$ ,  $\text{Fe}_{78}\text{Si}_9\text{B}_{13}$ ,  $\text{Co}_{68}\text{Cu}_{23}\text{B}_9$  and  $\text{Fe}_{64}\text{Nb}_{28}\text{B}_8$  by high energy milling (HEM) for applications of synthetic biomaterials in bone tissue regeneration. However, the use of the amorphous alloys  $\text{Co}_{69}\text{Nb}_{23}\text{B}_8$ ,  $\text{Fe}_{78}\text{Si}_9\text{B}_{13}$ ,  $\text{Co}_{68}\text{Cu}_{23}\text{B}_9$  and  $\text{Fe}_{64}\text{Nb}_{28}\text{B}_8$ , synthesized by high energy milling (HEM), is being used for biomedical

field. Then, their physical-chemical, magnetic, thermal, mechanical and biological properties were evaluated, in addition to their viability for application in the biomedical field.

## 2. Material and method:

Elemental metal powders (99.9% purity, from Êxodo Científica – LTDA/Brazil) of Co, Fe, Nb, Cu, Si and B with nominal compositions of amorphous alloys Co<sub>69</sub>Nb<sub>23</sub>B<sub>8</sub>, Fe<sub>78</sub>Si<sub>9</sub>B<sub>13</sub>, Co<sub>68</sub>Cu<sub>23</sub>B<sub>9</sub> and Fe<sub>64</sub>Nb<sub>28</sub>B<sub>8</sub> (in at. %) were mechanically ground in a planetary ball mill (Fritsch Pulverisette 5). The powder mixture load was maintained at 20 g for all tests, as well as the ball-to-powder ratio by weight of 20:1. The test speed adopted was 300 rpm and a grinding time of 15 h. Finally, ethyl alcohol (C<sub>2</sub>H<sub>6</sub>O) (2 mL) was used as a process control agent (PCA) in the grinding medium to regulate the morphology of the homogenized powder and an argon atmosphere. The microstructural evaluation of the samples obtained from the mechanical alloy was performed by X-ray diffraction (XRD; BRUKER diffractometer, model D2 Phaser) using CuK $\alpha$  radiation ( $\lambda = 1.54056 \text{ \AA}$ ) produced at 45 kV and 40 mA. The diffraction angle ( $2\theta$ ) varied between  $10^\circ$  and  $80^\circ$  with a step of  $0.012^\circ$  and a time of 5 s. A TESCAN scanning electron microscope, model VEGA 3, operating in the voltage range of 5 or 10 kV, was used for the microstructural characterization. The samples were placed on a metal support (stage) and previously coated with a thin layer of gold (Au). Then, images were obtained at different points of the samples and at magnification in the order of 100 kx. From the analysis of the images, it was possible to observe the surface morphological modifications in the amorphous alloys Co<sub>69</sub>Nb<sub>23</sub>B<sub>8</sub>, Fe<sub>78</sub>Si<sub>9</sub>B<sub>13</sub>, Co<sub>68</sub>Cu<sub>23</sub>B<sub>9</sub> and Fe<sub>64</sub>Nb<sub>28</sub>B<sub>8</sub>. The thermal studies of the amorphous powders of Co<sub>69</sub>Nb<sub>23</sub>B<sub>8</sub>, Fe<sub>78</sub>Si<sub>9</sub>B<sub>13</sub>, Co<sub>68</sub>Cu<sub>23</sub>B<sub>9</sub> and Fe<sub>64</sub>Nb<sub>28</sub>B<sub>8</sub> were collected after grinding, using differential thermal analysis (DTA) and thermogravimetric analysis (TGA) equipment from SHIMADZU DTG-60H. All thermal studies were conducted under an argon atmosphere with a heating rate of  $10^\circ\text{C}/\text{min}$ . The textural analysis was performed using a Quantachrome NOVA 2200E BET surface area and pore size analyzer, Autosorb IQ model, to obtain adsorption/desorption isotherms of the amorphous alloys Co<sub>69</sub>Nb<sub>23</sub>B<sub>8</sub>, Fe<sub>78</sub>Si<sub>9</sub>B<sub>13</sub>, Co<sub>68</sub>Cu<sub>23</sub>B<sub>9</sub> and Fe<sub>64</sub>Nb<sub>28</sub>B<sub>8</sub>. The uniaxial compressive mechanical tests were conducted in a WDW-100 testing machine at a deformation rate of  $4 \cdot 10^{-4} \text{ s}^{-1}$  at room temperature. The powder sizes of the alloys Co<sub>69</sub>Nb<sub>23</sub>B<sub>8</sub>, Fe<sub>78</sub>Si<sub>9</sub>B<sub>13</sub>, Co<sub>68</sub>Cu<sub>23</sub>B<sub>9</sub> and Fe<sub>64</sub>Nb<sub>28</sub>B<sub>8</sub> were pressed into cylindrical disc shapes and are 2 mm in diameter and 4 mm in height. Compression tests were performed at least in triplicate for the amorphous powders Co<sub>69</sub>Nb<sub>23</sub>B<sub>8</sub>, Fe<sub>78</sub>Si<sub>9</sub>B<sub>13</sub>, Co<sub>68</sub>Cu<sub>23</sub>B<sub>9</sub> and Fe<sub>64</sub>Nb<sub>28</sub>B<sub>8</sub>. The magnetic properties were studied by a vibrating sample magnetometer (VSM) at room temperature of  $25^\circ\text{C}$  and a magnetic field in the range of  $\pm 40 \text{ kOe}$ . The cell viability assay by MTT for the amorphous alloys Co<sub>69</sub>Nb<sub>23</sub>B<sub>8</sub>, Fe<sub>78</sub>Si<sub>9</sub>B<sub>13</sub>, Co<sub>68</sub>Cu<sub>23</sub>B<sub>9</sub> and Fe<sub>64</sub>Nb<sub>28</sub>B<sub>8</sub>, performed using the MTT assay with MC3T3 osteoblastic cells, showed a cytotoxic profile that, at the safe concentration, the cell viability was higher than 70%, promising potential for applicability as metallic biomaterial for biomedicine.

## 3. Results and Discussion:

**Figure 1** shows the diffractograms of the alloys Co<sub>69</sub>Nb<sub>23</sub>B<sub>8</sub> (a), Co<sub>68</sub>Cu<sub>23</sub>B<sub>9</sub> (b), Fe<sub>64</sub>Nb<sub>28</sub>B<sub>8</sub> (c) and Fe<sub>78</sub>Si<sub>9</sub>B<sub>13</sub> (d) processed by mechanical grinding (HEM). In the diffractograms, in the  $2\theta$  range of  $40^\circ - 50^\circ$ , a typical diffuse halo is observed, with no indication of an obvious diffraction peak corresponding to the crystalline phases, as shown in the central part inside the red dashed circle, characteristic of an amorphous structure.

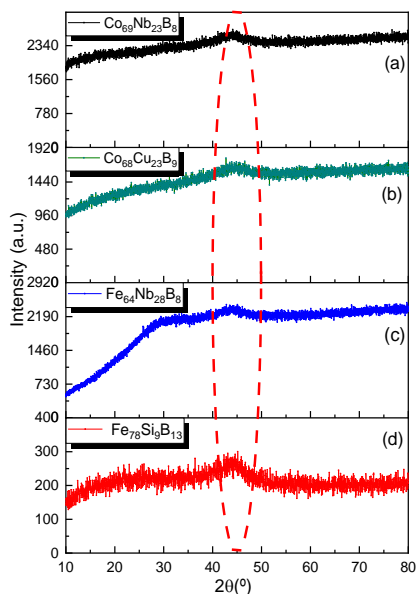


**Figure 1.** X-ray diffraction patterns of the amorphous alloys  $\text{Co}_{69}\text{Nb}_{23}\text{B}_8$  (a),  $\text{Co}_{68}\text{Cu}_{23}\text{B}_9$  (b),  $\text{Fe}_{64}\text{Nb}_{28}\text{B}_8$  (c) and  $\text{Fe}_{78}\text{Si}_9\text{B}_{13}$  (d).

**Figure 2** illustrates the vibrational spectra of the amorphous alloys  $\text{Co}_{69}\text{Nb}_{23}\text{B}_8$  (a),  $\text{Co}_{68}\text{Cu}_{23}\text{B}_9$  (b),  $\text{Fe}_{64}\text{Nb}_{28}\text{B}_8$  (c) and  $\text{Fe}_{78}\text{Si}_9\text{B}_{13}$  (d) obtained by HEM in the infrared region of  $4000 - 500 \text{ cm}^{-1}$ .

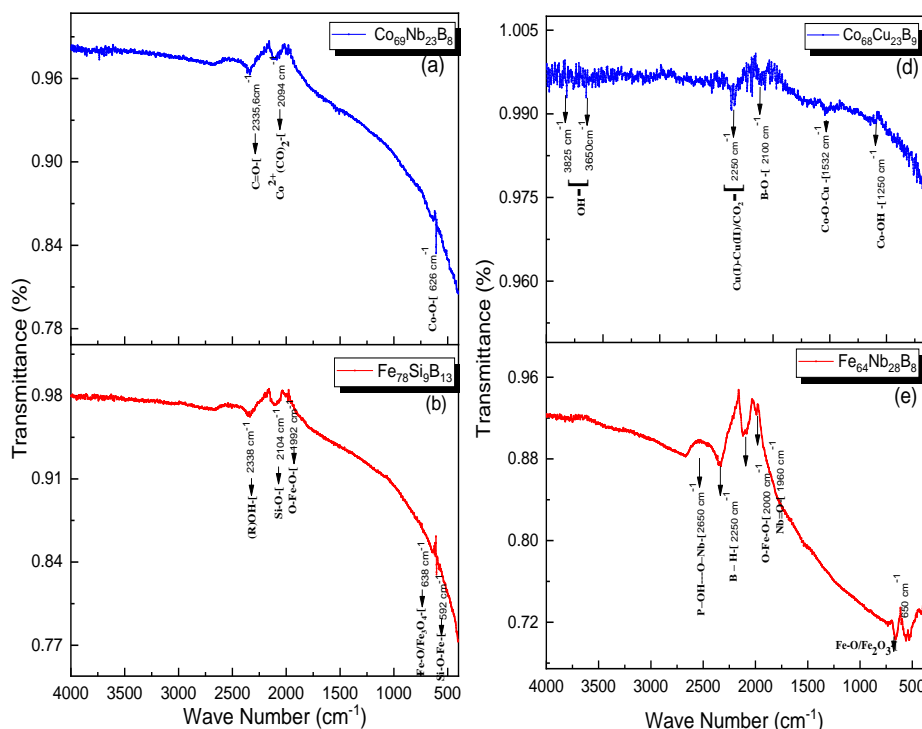


**Figure 2.** FTIR spectra of the amorphous alloys  $\text{Co}_{69}\text{Nb}_{23}\text{B}_8$  (a),  $\text{Co}_{68}\text{Cu}_{23}\text{B}_9$  (b),  $\text{Fe}_{64}\text{Nb}_{28}\text{B}_8$  (c) and  $\text{Fe}_{78}\text{Si}_9\text{B}_{13}$  (d).

The FTIR spectra of the amorphous alloy  $\text{Co}_{69}\text{Nb}_{23}\text{B}_8$  (a) showed a band at  $\sim 2335.6 \text{ cm}^{-1}$ , which is attributed to the stretching vibration modes of the C=O group of atmospheric  $\text{CO}_2$  [26]. The FTIR absorption spectrum in the vicinity of  $\sim 2094 \text{ cm}^{-1}$  slightly decreases in intensity, which is most likely due to the formation of some dicarbonyl  $\text{Co}^{2+}(\text{CO})_2$  species

absorbing at lower frequencies [27]. The band observed at  $626\text{ cm}^{-1}$  is attributed to the stretching frequency of Co-O, where Co is  $\text{Co}^{2+}$  and is tetrahedrally coordinated due to the presence of the spinel of  $\text{Co}_3\text{O}_4$  [28].

Analyzing the FTIR spectrum of the amorphous alloy  $\text{Fe}_{78}\text{Si}_9\text{B}_{13}$  (b) it can be observed that the absorption band observed at  $2338\text{ cm}^{-1}$  corresponds to the presence of (R)O-H groups (R = Si and B or Ba), for example, the silanol group SiOH [29]. A broad band was observed in the region of  $2104\text{ cm}^{-1}$  corresponding to the characteristic stretching mode of the Si-O group [30].

The band that appears around  $1992\text{ cm}^{-1}$  corresponds to the O-Fe-O stretching mode of  $\text{Fe}_2\text{O}_3$  [31]. The band at  $638\text{ cm}^{-1}$  represents the stretching vibration of the Fe-O bond in  $\text{Fe}_3\text{O}_4$  [32]. The occurrence of a band at  $592\text{ cm}^{-1}$  is attributed to the stretching vibrational mode of the Si-O-Fe group [33]. The bands at  $3825\text{ cm}^{-1}$  and  $3650\text{ cm}^{-1}$  in the FTIR spectrum of the  $\text{Co}_{68}\text{Cu}_{23}\text{B}_9$  (c) alloy are attributed to the axial stretching mode of the O-H group, due to the  $\text{H}_2\text{O}$  molecules having an incompletely developed hydrogen bond [34].

The presence of a band at  $2250\text{ cm}^{-1}$  indicates the involvement of unstable oxidation processes of Cu(I) to Cu (II) ions, which can be attributed to vibrations caused by atmospheric  $\text{CO}_2$  [35]. The band around  $2100\text{ cm}^{-1}$  is due to the stretching vibrations of the B-O bonds of  $\text{BO}_3^-$ , which involves the bonding of different oxygen groups [36].

The FTIR band at  $1532\text{ cm}^{-1}$  can be attributed to a metal-metal charge transfer exclusive to the oxo-bridged Co-O-Cu bond in the octahedral coordination [104]. The absorption spectra in the  $1250\text{ cm}^{-1}$  range are attributed to the stretching of non-bridged oxygen atoms of the Co-OH type [37]. Regarding the FTIR band around  $2650\text{ cm}^{-1}$  of the amorphous alloy  $\text{Fe}_{64}\text{Nb}_{28}\text{B}_8$  (d) is directly related to the presence of niobium. The nature of this band cannot be clearly established, but it may be related to the formation of P-OH...O-Nb bridges instead of P-OH...O-P [38].

This vibration becomes narrower as the niobium oxide content increases. The evolution of this band indicates that in addition to a decrease in the amount of OH, niobium oxide changes the nature of the OH bond and, therefore, the associated vibration frequency [39]. The band observed at  $\sim 2250\text{ cm}^{-1}$  in the  $\text{Fe}_{64}\text{Nb}_{28}\text{B}_8$  alloy (d) is caused by the stretching vibration modes of the B-H group [49].

The band around  $2000\text{ cm}^{-1}$  is attributed to the asymmetric stretching vibrations of the O-Fe-O group [41]. The FTIR spectrum showed the presence of a strong band at  $\sim 1960\text{ cm}^{-1}$ , being attributed to the stretching vibration mode of Nb=O [42,43]. Furthermore, the strong absorption band at  $650\text{ cm}^{-1}$  reported in the FTIR spectrum of the amorphous alloy is attributed to the stretching vibrations of Fe-O and  $\text{Fe}_2\text{O}_3$  bonds [44].

All absorptions and assignments related to the amorphous alloys  $\text{Co}_{69}\text{Nb}_{23}\text{B}_8$  (a),  $\text{Co}_{68}\text{Cu}_{23}\text{B}_9$  (b),  $\text{Fe}_{64}\text{Nb}_{28}\text{B}_8$  (c) and  $\text{Fe}_{78}\text{Si}_9\text{B}_{13}$  (d) are described in **Table 1**.

**Table 1.** Wavenumber and absorption bands for the amorphous alloys  $\text{Co}_{69}\text{Nb}_{23}\text{B}_8$  (a),  $\text{Co}_{68}\text{Cu}_{23}\text{B}_9$  (b),  $\text{Fe}_{64}\text{Nb}_{28}\text{B}_8$  (c) and  $\text{Fe}_{78}\text{Si}_9\text{B}_{13}$  (d).

Amorphous alloys	Wave number ( $\text{cm}^{-1}$ )	Assignment
	$\sim 2335,6$	Stretching vibration modes of the C=O group of atmospheric $\text{CO}_2$
$\text{Co}_{69}\text{Nb}_{23}\text{B}_8$ (a)	$\sim 2094$	Formation of dicarbonyl species
	$\sim 626$	Attributed to the Co-O stretching frequency
	2338	Presence of (R)O-H groups (R= Si and B or Ba)
	2104	Si-O group stretching mode
$\text{Fe}_{78}\text{Si}_9\text{B}_{13}$ (b)	1992	O-Fe-O stretching mode of $\text{Fe}_2\text{O}_3$
	638	Stretching vibration of the Fe-O bond in $\text{Fe}_3\text{O}_4$ stretching
	592	Presence of stretching vibration of the Si-O-Fe group -
	3825-3650	Axial stretching mode of the O-H group
	2250	Oxidation of Cu(I) ions to Cu (II) due to atmospheric $\text{CO}_2$
$\text{Co}_{68}\text{Cu}_{23}\text{B}_9$ (c)	2100	Stretching vibrations of the B-O bonds of $\text{BO}_3^-$
	1532	Assigned to the oxo-bridge bond Co-O-Cu
	1250	Co-OH type stretching
	2650	Formation of P-OH...O-Nb bridges
	$\sim 2250$	B-H group stretching vibrations
$\text{Fe}_{64}\text{Nb}_{28}\text{B}_8$ (d)	2000	Asymmetric stretching of the O-Fe-O group
	$\sim 1960$	Stretching vibration of Nb=O
	650	Stretching of Fe-O and $\text{Fe}_2\text{O}_3$

**Figure 3** illustrates the micrographs of the amorphous alloys a)  $\text{Co}_{69}\text{Nb}_{23}\text{B}_8$ , b)  $\text{Co}_{68}\text{Cu}_{23}\text{B}_9$ , c)  $\text{Fe}_{78}\text{Si}_9\text{B}_{13}$  and d)  $\text{Fe}_{64}\text{Nb}_{28}\text{B}_8$  obtained by SEM. The micrographs of each amorphous alloy give an idea of the morphological structure of the amorphous powders and were grouped with a scale of 50  $\mu\text{m}$  and a magnification of 100kx.

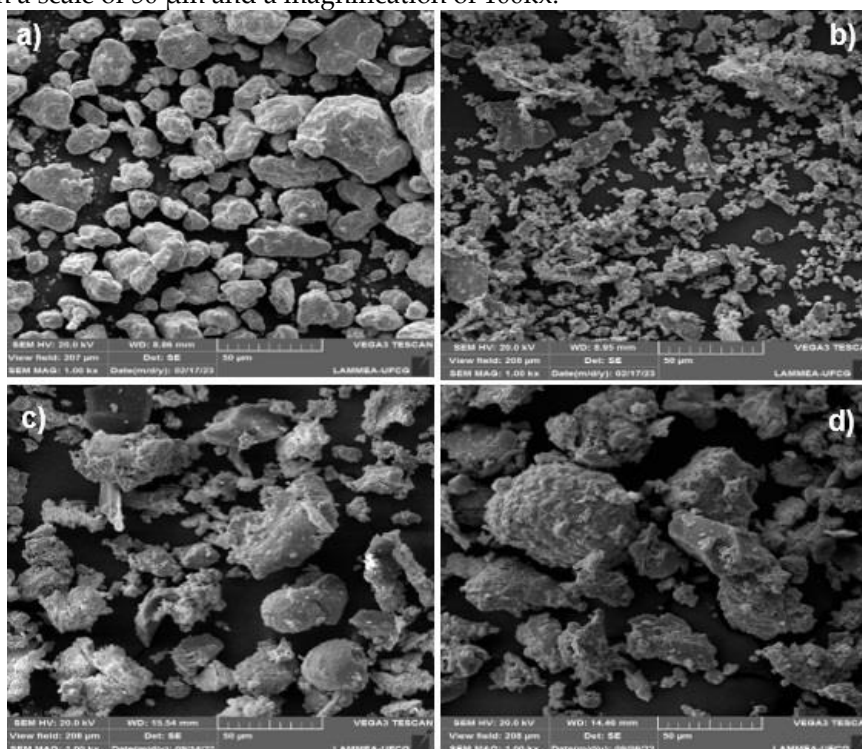


**Figure 3.** Micrographs obtained by SEM of amorphous alloys a)  $\text{Co}_{69}\text{Nb}_{23}\text{B}_8$ , b)  $\text{Co}_{68}\text{Cu}_{23}\text{B}_9$ , c)  $\text{Fe}_{78}\text{Si}_9\text{B}_{13}$  and d)  $\text{Fe}_{64}\text{Nb}_{28}\text{B}_8$ .

In the micrograph of **Figure 3 a)**  $\text{Co}_{69}\text{Nb}_{23}\text{B}_8$ , an agglomeration of particles with irregular and very flattened morphology is observed, which occurs due to the plastic deformation and ductility of the powders that undergo hardening and bonding by crushing, resulting in final particles with irregular morphology and non-uniform size [45]. In this case, the particle size increased with irregular shape and produced a mixture with a wide particle size distribution of 50  $\mu\text{m}$  [46].

The amorphous powder particles in b)  $\text{Co}_{68}\text{Cu}_{23}\text{B}_9$  were milled for 15 h to reach a size of 50  $\mu\text{m}$ , which shows an irregular particle morphology, typical of small flakes that transform into fine particles due to the plastic deformation of the  $\text{Co}_{68}\text{Cu}_{23}\text{B}_9$  alloy powder during high-energy milling [47].

The representative SEM micrograph of the amorphous alloy c)  $\text{Fe}_{78}\text{Si}_9\text{B}_{13}$  shows that the powders are hardened by intense plastic deformation during grinding, becoming brittle in nature. In this case, irregular agglomeration and cold welding occur over fracturing mechanisms. Thus, the particle size is reduced and a mixture of hemispherical particles with a narrow size distribution of 50  $\mu\text{m}$  is developed [48]. In this way, a more homogenized and very uniform mixture was obtained. As shown in the micrograph of the powder of the amorphous alloy d)  $\text{Fe}_{64}\text{Nb}_{28}\text{B}_8$ , it is clear that it presents an irregular agglomeration morphology with a uniform and homogeneous distribution, due to the numerous fractures and reduction of particles with a size of 50  $\mu\text{m}$  due to the cold-welding process, presenting very few pores on its surface [49]. The balance between fracture and cold welding of powder particles is assisted by the high contact pressure between the spheres and powders, as well as between the spheres and vials, leading to the creation of new surfaces that come into contact with each other under significant plastic deformation.

This results in the flattening of the powder particles and the emergence of a varied and irregular morphology [50]. Continuous milling led to a combination of continuous fracturing and cold-welding processes, resulting in aggregates of smaller particles with irregular shapes and particle sizes of 50  $\mu\text{m}$  during the 15 h of milling. Thus, it can be stated that this caused the fracture to occur more abruptly.

**Figure 4** illustrates the thermal events observed from the superimposed TGA/DTA curves for the amorphous alloys  $\text{Co}_{69}\text{Nb}_{23}\text{B}_8$  (a),  $\text{Co}_{68}\text{Cu}_{23}\text{B}_9$  (b),  $\text{Fe}_{64}\text{Nb}_{28}\text{B}_8$  (c) and  $\text{Fe}_{78}\text{Si}_9\text{B}_{13}$  (d), which allows the determination of the decomposition temperatures ( $^{\circ}\text{C}$ ), transformation of amorphous phases and mass losses.

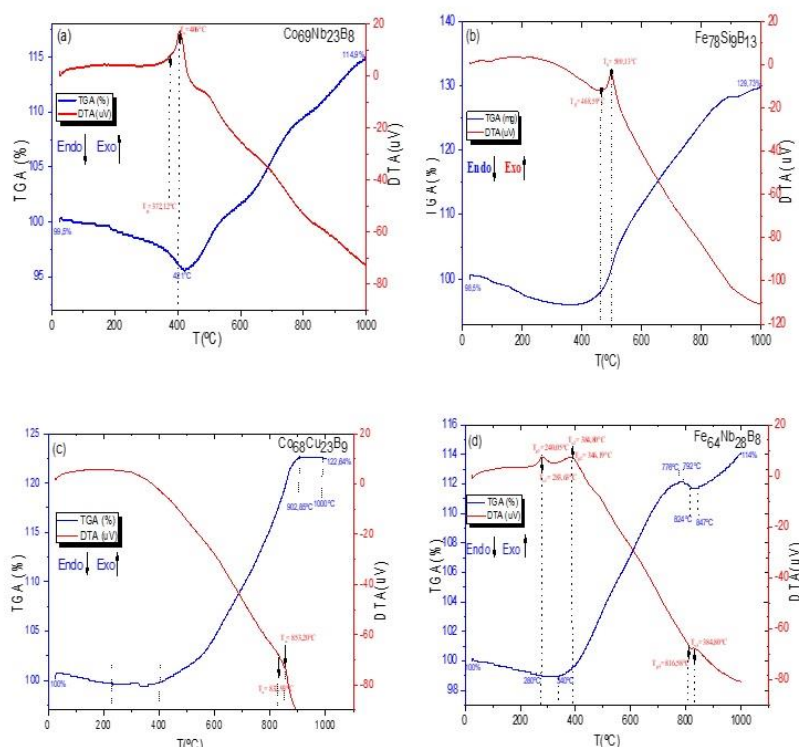


**Figure 4.** Superimposed TGA/DTA curves of the amorphous alloys  $\text{Co}_{69}\text{Nb}_{23}\text{B}_8$  (a),  $\text{Co}_{68}\text{Cu}_{23}\text{B}_9$  (b),  $\text{Fe}_{64}\text{Nb}_{28}\text{B}_8$  (c) and  $\text{Fe}_{78}\text{Si}_9\text{B}_{13}$  (d).

In the TGA curve in **Figure 4 a)** referring to the  $\text{Co}_{69}\text{Nb}_{23}\text{B}_8$  alloy, the TGA curve has endothermic behavior up to a temperature of  $\sim 421^\circ\text{C}$ , representing a mass loss of  $\sim 3.65\%$ . The exothermic peak in the DTA curve, located around  $406^\circ\text{C}$ , is possibly associated with some crystallization or phase transformation process, or even followed by high-temperature oxidation with some mass gains [51,52]. Compared with other similar amorphous alloys, B in the alloy composition effectively increases the crystallization temperature and its thermal stability.

According to **Figure 4 a)**, the glass transition temperature is  $T_g=372.12^\circ\text{C}$  and the first crystallization temperature is around  $T_x=406^\circ\text{C}$  for the amorphous alloy  $\text{Co}_{69}\text{Nb}_{23}\text{B}_8$  (a), which corresponds to the supercooled liquid region corresponding to the endothermic peak used, which is considered a good indicator of thermal stability, since the higher value of  $\Delta T$  causes a delay in the nucleus, that is,  $\Delta T=T_x-T_g=33.88^\circ\text{C}$  with amorphous alloys/bulk metal glasses (BMG) [53,54]. At higher temperatures, Co ions such as Nb are oxidized by the environment and therefore the mass can be slightly increased to 114.9% (see **Figure 4 a)**). It is assumed that the grain size may have increased since the ionic radius of Co ( $0.65\text{\AA}$ ) is larger than that of Nb ( $\approx 0.62\text{\AA}$ ) (Lee, 1999).

The measurements of the superimposed TGA/DTA curves of the  $\text{Fe}_{78}\text{Si}_9\text{B}_{13}$  alloy in **Figure 4 b)** show the DTA curve exhibiting a single exothermic peak for crystallization of the supercooled liquid at  $500.13^\circ\text{C}$  ( $T_x$ ). In amorphous alloys or even in amorphous materials, there is a glass transition behavior prior to crystallization. In **Figure 4 b)** for the  $\text{Fe}_{78}\text{Si}_9\text{B}_{13}$  alloy, an endothermic peak corresponding to the glass transition of  $468.59^\circ\text{C}$  ( $T_g$ ) and the supercooled liquid region can be observed, which is considered a good indicator of thermal stability, since a higher value of  $\Delta T$  causes a delay in nucleation, that is,  $\Delta T=T_x-T_g=31.54^\circ\text{C}$ , for amorphous alloys/bulk metallic glasses (BMG - Bulk Metallic Glasses) [55,56]. At higher temperatures, both the Fe and Si ions of the TGA are oxidized by the environment, so that the mass easily increases to 129.73% as shown in **Figure 4 b)**. The increase in grain size is due to high-temperature oxidation, which led to a greater increase in the ionic radius of Fe ( $0.78\text{\AA}$ ) than that of Si ( $\approx 0.26\text{\AA}$ ) [57].

In the amorphous alloy  $\text{Co}_{68}\text{Cu}_{23}\text{B}_9$  in **Figure 4c**), it is observed that at  $T_x=853.20^\circ\text{C}$  there is a small formation of a small exothermic peak for the crystallization of the supercooled liquid, followed by a low glass transition temperature of  $T_g=832.93^\circ\text{C}$  (almost imperceptible in the graph in **Figure 4c**)). This reveals a residual increase in the amorphous phase at  $850^\circ\text{C}$ , due to the decrease in crystallization in this last exothermic peak [58].

The value of  $\Delta T$  causes a delay in the growth of the grain nucleus, that is,  $\Delta T = T_x - T_g = 20.27^\circ\text{C}$  shows a good indicator of thermal stability, with this type of stoichiometry of the amorphous alloy  $\text{Co}_{68}\text{Cu}_{23}\text{B}_9$  [59]. It is also noted that there is a reactive step at the thermal decomposition temperature that is relatively high, between  $902.85^\circ\text{C}$  and  $1000^\circ\text{C}$ , which shows good thermal stability properties indicating that the mass becomes constant in this temperature range. Co ions like Cu ions are oxidized by the environment and, therefore, there is a drastic increase in mass to 122.64% in the TGA curve of  $\text{Co}_{68}\text{Cu}_{23}\text{B}_9$  as illustrated in **Figure 4 c**).

**Figure 4d**) illustrates the thermal events observed from the superimposed TGA/DTA curves for the  $\text{Fe}_{64}\text{Nb}_{28}\text{B}_8$  alloy, where two exothermic peaks can be observed. The first peak is caused by the crystallization of the bcc-Fe(Nb) phase, and the second peak is due to the crystallization of  $\text{Fe}_2\text{B}$  and  $\text{Fe}_3\text{B}$  phases that act as an inhomogeneous nucleation site diluted with the amorphous phase that is related to the structural relaxation that occurs just before the glass transition, resulting in a generally low characteristic temperature before the phases form [60,61].

The first and second crystallization temperatures  $T_{x1}$  and  $T_{x2}$ , which are determined by the onset of the DTA peaks, are  $T_{x1} = 283.63^\circ\text{C}$  and  $T_{x2} = 384.80^\circ\text{C}$ , which, followed by their glass transition temperatures, are  $T_{g1} = 240.05^\circ\text{C}$  and  $T_{g2} = 346.19^\circ\text{C}$ , respectively. In addition, the values of  $\Delta T_1 = T_{x1} - T_{g1} = 43.58^\circ\text{C}$  and  $\Delta T_2 = T_{x2} - T_{g2} = 38.61^\circ\text{C}$  cause a delay in the grain nucleus, that is, creating thermal stability for amorphous alloys/bulk metal glasses (BMG - Bulk Metal Glasses) [62].

According to **Figure 4d**), the TGA curve has a first small high step in the first temperature range from  $776$  to  $792^\circ\text{C}$  and in the second step, a temperature range between  $824$  and  $847^\circ\text{C}$ , presenting in both a relatively high thermal decomposition. Figure 5 shows the results of the textural characterization of the amorphous alloys  $\text{Co}_{69}\text{Nb}_{23}\text{B}_8$  (a),  $\text{Fe}_{78}\text{Si}_9\text{B}_{13}$  (b),  $\text{Co}_{68}\text{Cu}_{23}\text{B}_9$  (c) and  $\text{Fe}_{64}\text{Nb}_{28}\text{B}_8$  (d) obtained by HEM by  $\text{N}_2$  adsorption/desorption isotherms.

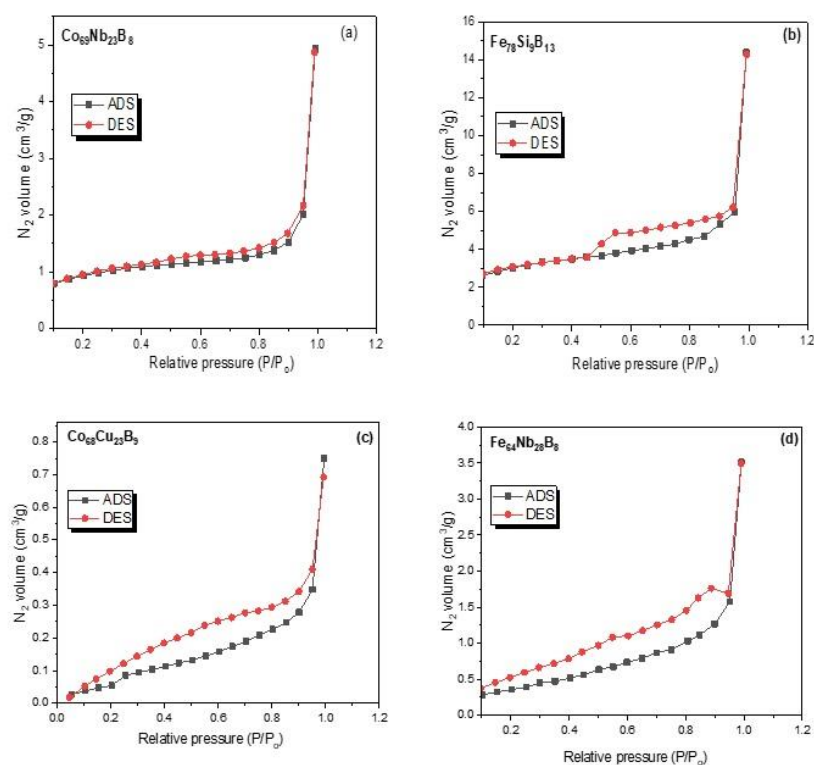


**Figure 5.** N<sub>2</sub> adsorption/desorption isotherms for amorphous alloys Co<sub>69</sub>Nb<sub>23</sub>B<sub>8</sub> (a), Fe<sub>78</sub>Si<sub>9</sub>B<sub>13</sub> (b), Co<sub>68</sub>Cu<sub>23</sub>B<sub>9</sub> (c) and Fe<sub>64</sub>Nb<sub>28</sub>B<sub>8</sub> (d).

Thus, the amorphous alloys Co<sub>69</sub>Nb<sub>23</sub>B<sub>8</sub> (a), Fe<sub>78</sub>Si<sub>9</sub>B<sub>13</sub> (b), Co<sub>68</sub>Cu<sub>23</sub>B<sub>9</sub> (c) and Fe<sub>64</sub>Nb<sub>28</sub>B<sub>8</sub> (d) presented surface structures with an adsorption isotherm curve profile, which according to IUPAC - International Union of Pure and Applied Chemistry, fall into type V [63], suggesting a mesoporous characteristic of the materials (pore size in the range of 10–250 Å) and an ordered arrangement of pores giving it a well-ordered structure [64,64]. At the same time, analyzing the hysteresis shapes corresponding to the different pore geometries, it can be observed that these amorphous alloys are represented by type 3 (H3) hysteresis loops (formation of wedge-shaped pores, parallel cones or plate-shaped pores) [65]. The presence of the hysteresis loop indicates that mesopores also accompany the micropores. This phenomenon has been established for activated carbons prepared under low nitrogen flow rates (500°C) [66].

Thus, it can be concluded that these moderate carbonization conditions are a contribution to the mesopores. The pores present in these amorphous alloys are important for orthopedic biomedical applications. Based on **Figure 5**, typical isotherms for mesoporous solids are observed, and are characterized by a very sharp hysteresis loop between the adsorption and desorption branches for amorphous alloys.

In addition, a very significant hysteresis can appear in the adsorption and desorption branches, as they also do not return to the origin. It is observed that the absence of limitation of the adsorbed amount of N<sub>2</sub> is saturated at high values of P/P<sub>0</sub>, indicating a strong tendency for a mesoporous material [66,67]. It is observed in the isotherms of amorphous alloys that the inflection point in the hysteresis occurs around P/P<sub>0</sub> = 0.4-1, which is typically a characteristic of the existence of strong mesoporosity and an adsorption and desorption cycle. Mesoporous phases with medium and large pores were observed in the same range of P/P<sub>0</sub> = 0.8-1 [68] in **Figure 5**.

The relative pressure (P/P<sub>0</sub>) in the separated region in the adsorption and desorption curves was greater than 0.8 in the amorphous alloys in which larger pore diameters were observed. The hysteresis was caused by the high capillary condensation that occurred in the mesopores [69]. The desorption hysteresis curve H3 contains a slope associated with

a force in the hysteresis loop, due to the so-called tensile strength effect (this phenomenon perhaps occurs for  $N_2$  at 77 K in the relative pressure range of 0.4 to 0.45). In conclusion, the isotherms of the amorphous alloys are similar to each other and present the same type IV isotherm and H3 curve of the hysteresis loop. The isotherms presented a hysteresis loop of type H3. This hysteresis typology is characteristic and normally associated with non-rigid aggregates of plate-shaped particles, originating slit pores. It is characterized by presenting different evaporation and condensation paths between the adsorption and desorption processes undergone by the adsorbent materials.

In summary, the isotherms for the amorphous alloys  $Co_{69}Nb_{23}B_8$  (a),  $Fe_{78}Si_9B_{13}$  (b),  $Co_{68}Cu_{23}B_9$  (c) and  $Fe_{64}Nb_{28}B_8$  (d) are similar to each other and presented the same type IV isotherm profile and H3 hysteresis loop. The measured specific surface areas of the amorphous alloys  $Co_{69}Nb_{23}B_8$  (a),  $Fe_{78}Si_9B_{13}$  (b),  $Co_{68}Cu_{23}B_9$  (c) and  $Fe_{64}Nb_{28}B_8$  (d) are 3.215, 4.237, 3.121 and 4.201  $m^2 g^{-1}$  respectively. These values are in good agreement with the results reported [70], when they developed new amorphous alloy catalysts of Ni–P (R–Ni–P), Ni–Co–B, and Ni–B (P)/ $SiO_2$  type for Fischer-Tropsch process in catalytic hydrogenation reactions of various organic compounds. On the other hand, the average pore diameter values for the amorphous alloys  $Co_{69}Nb_{23}B_8$  (a),  $Fe_{78}Si_9B_{13}$  (b),  $Co_{68}Cu_{23}B_9$  (c) and  $Fe_{64}Nb_{28}B_8$  (d) were 3.16, 4.19, 3.14 and 4.18 nm, respectively, which are relatively close values compared to published works [71,72], when studying the morphological characteristics of other amorphous alloy compositions.

The mesoporous nature of these amorphous alloys obtained by HEM is confirmed by the particle volume and diameter values, which range from 2 to 50 nm according to the IUPAC classification that characterizes mesoporous materials [73,74].

Pore volume and particle size are fundamental parameters for studying the structure and porosity of these amorphous alloys, since they are related to their total area, which can serve as a reaction substrate in biomaterials. **Figure 6** illustrates the behavior of magnetization (M) as a function of the applied coercive field (H) through hysteresis loops for the amorphous alloys  $Co_{69}Nb_{23}B_8$  (a),  $Fe_{78}Si_9B_{13}$  (b),  $Co_{68}Cu_{23}B_9$  (c) and  $Fe_{64}Nb_{28}B_8$  (d), which were obtained by HEM.

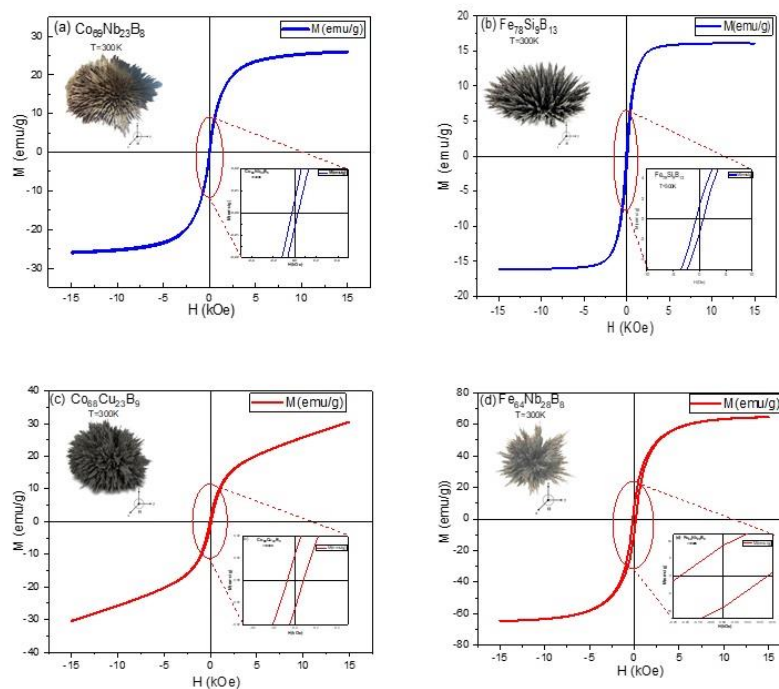


**Figure 6.** M x H hysteresis curves for amorphous alloys  $Co_{69}Nb_{23}B_8$  (a),  $Fe_{78}Si_9B_{13}$  (b),  $Co_{68}Cu_{23}B_9$  (c) e  $Fe_{64}Nb_{28}B_8$  (d).

The  $M \times H$  hysteresis loops of  $\text{Co}_{69}\text{Nb}_{23}\text{B}_8$  (a),  $\text{Fe}_{78}\text{Si}_9\text{B}_{13}$  (b),  $\text{Co}_{68}\text{Cu}_{23}\text{B}_9$  (c) e  $\text{Fe}_{64}\text{Nb}_{28}\text{B}_8$  (d) show the estimated saturation magnetizations of  $M_s = 15.023$  emu/g,  $M_s = 18.932$  emu/g,  $M_s = 15.021$  emu/g and  $M_s = 18.832$  emu/g, remanent magnetizations of  $M_r = 0.01603$  emu/g,  $M_r = 0.01820$  emu/g,  $M_r = 0.01525$  emu/g and  $M_r = 0.01819$  emu/g, and the estimated coercive fields of  $H_c = 70.86$  kOe,  $H_c = 77.82$  kOe,  $H_c = 70.14$  kOe and  $H_c = 77.81$  kOe. In the upper part of **Figure 6**, it was observed that the amorphous alloys have hysteresis curves of ferrimagnetic behavior, which are characteristic of soft magnetic materials, which magnetize and demagnetize at low field values, due to their small values of remanent magnetization and coercivity, but different from zero, thus revealing the complete formation of the narrow magnetic hysteresis cycle after grinding the powder for 15 h. The remanence/saturation ratio ( $M_r/M_s$ ) varied in the range of 0.000081 to 0.001066. However, the  $M_r/M_s$  ratio defines the degree of quadrature of the hysteresis loop of a magnetic material, providing information about how well the material retains its magnetization when an external magnetic field is applied and removed. It is an insightful criterion to assess the domain state, distinguishing between single domains ( $M_r/M_s > 0.5$ ) and multidomains ( $M_r/M_s \ll 0.1$ ) [75]. A value of  $M_r/M_s \ll 0.1$  indicates that the powder particles are multidomains where the magnetization modification may be due to the domain wall motion at relatively low fields. This means that amorphous alloys produced through MAE present multidomains compared to other metallic alloy systems that are based on Bloch domain wall models and uniaxial anisotropic ferromagnetic particles that are randomly oriented with domains very close to ( $\sim 0.5$ ) [76,77]. Generally, in mechanically milled amorphous alloys, the remanence/saturation ratio ( $M_r/M_s$ ) value is usually very low, between 0.001 and 0.1 [78,79]. However, on the other hand, extrinsic characteristics such as grain and/or particle size directly influence magnetic multidomains and can contribute to increased magnetization, since the larger the particle and/or grain size, the lower the energy level, favoring greater magnetization [80]. **Figure 7** illustrates the typical compressive stress-strain curves for the amorphous alloys  $\text{Co}_{69}\text{Nb}_{23}\text{B}_8$  (a),  $\text{Fe}_{78}\text{Si}_9\text{B}_{13}$  (b),  $\text{Co}_{68}\text{Cu}_{23}\text{B}_9$  (c) e  $\text{Fe}_{64}\text{Nb}_{28}\text{B}_8$  (d).

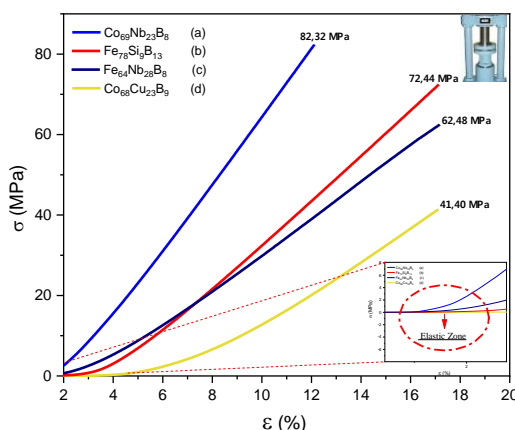


**Figure 7.** Stress-strain curves of mechanical tests of compressive strength of amorphous alloys  $\text{Co}_{69}\text{Nb}_{23}\text{B}_8$  (a),  $\text{Fe}_{78}\text{Si}_9\text{B}_{13}$  (b),  $\text{Co}_{68}\text{Cu}_{23}\text{B}_9$  (c) e  $\text{Fe}_{64}\text{Nb}_{28}\text{B}_8$  (d).

The amorphous alloy  $\text{Co}_{69}\text{Nb}_{23}\text{B}_8$  (a) as ground by mechanical grinding (HEM) exhibits a moderate elastic modulus of 6.80 MPa and a high yield strength of 82.37 MPa. The elastic modulus of the  $\text{Fe}_{78}\text{Si}_9\text{B}_{13}$  alloy (b) was 4.23 MPa and the yield strength was slightly higher at 72.44 MPa than that of the  $\text{Co}_{69}\text{Nb}_{23}\text{B}_8$  alloy (a). The  $\text{Co}_{68}\text{Cu}_{23}\text{B}_9$  alloy (d) has a very low elastic modulus of 2.42 MPa and yield strength of 41.40 MPa compared to other alloys. It is found that the amorphous alloy  $\text{Fe}_{64}\text{Nb}_{28}\text{B}_8$  (c) exhibits a moderate elastic modulus. The amorphous alloys studied here,  $\text{Co}_{69}\text{Nb}_{23}\text{B}_8$  (a),  $\text{Fe}_{78}\text{Si}_9\text{B}_{13}$  (b),  $\text{Co}_{68}\text{Cu}_{23}\text{B}_9$  (c) e  $\text{Fe}_{64}\text{Nb}_{28}\text{B}_8$  (d) did not show any fracture as can be observed after the elastic deformation stage of the curve measured at the strain rate of  $1 \cdot 10^{-4} \text{ s}^{-1}$  at room temperature [80]. In the

right corner inside the red circle, an increase in force is observed that corresponds to the linear elastic deformation zone of the material (slope of the linear elastic zone) during the initial compression phase of each alloy [81]. It should be noted that high elastic moduli correspond to materials with more pronounced elasticity. Although a test was performed for each amorphous alloy, only the best value for each composition was reported, since the lack of tension and friction homogeneity between the sample surface and the machine plates, due to imperfect plane parallelism in small samples, did not drastically alter the stress-strain response during the test. The compressive strength value of  $\text{Co}_{69}\text{Nb}_{23}\text{B}_8$  (a) is twice that of the  $\text{Co}_{68}\text{Cu}_{23}\text{B}_9$  alloy (d), but it is observed. Note that the  $\text{Co}_{69}\text{Nb}_{23}\text{B}_8$  alloy (a) has a lower deformation than the  $\text{Fe}_{78}\text{Si}_9\text{B}_{13}$  alloy (b). In fact, these values indicate that the  $\text{Co}_{69}\text{Nb}_{23}\text{B}_8$  alloy (a) is more resistant to mechanical stress and has a lower deformation capacity compared to  $\text{Fe}_{78}\text{Si}_9\text{B}_{13}$  (b), but in general it can be said that all amorphous alloys have good properties and are innovative materials and are being considered for biomedical applications due to their peculiar atomic structure in terms of amorphous phase and chemical composition.

In addition, amorphous alloys based on Co and Fe have excellent mechanical properties and corrosion resistance, which are directly related to cytocompatibility and biocompatibility for biomedical applications. Therefore, they can be directly applied in future studies, such as in vitro cellular studies, antimicrobial properties and in vivo studies in animals, such as in the area of human orthopedics and bone regeneration [82].

Although the compressive strength test was performed under the same conditions, only the best value of each alloy is provided here and, depending on the application, we can say that both amorphous alloys have better properties and can be applied in metallic biomaterial [83]. It is also observed that the amorphous alloy  $\text{Fe}_{64}\text{Nb}_{28}\text{B}_8$  (d) has a greater deformation, reaching twice, when compared to  $\text{Co}_{68}\text{Cu}_{23}\text{B}_9$  (c) [84]. This indicates that the sample  $\text{Fe}_{64}\text{Nb}_{28}\text{B}_8$  (d) has a compressive strength that is twice that of the other alloy  $\text{Co}_{68}\text{Cu}_{23}\text{B}_9$  (c). In practical terms, the sample  $\text{Fe}_{64}\text{Nb}_{28}\text{B}_8$  (d) resists more stress and also has a greater deformation capacity when compared to  $\text{Co}_{68}\text{Cu}_{23}\text{B}_9$  (c), but, depending on the application, they are said to have analogous properties [85]. Experimental results show that amorphous alloys based on Co and Fe obtained from the conventional milling process (HEM) present high elastic deformation and do not fracture [86]. These results indicate that the B and Si contents improve the resistance to deformation, therefore, the compression of these alloys is higher [87].

**Figure 8** Illustrated the data obtained in the MTT cell viability test for samples F1- $\text{Co}_{69}\text{Nb}_{23}\text{B}_8$ , F2- $\text{Fe}_{78}\text{Si}_9\text{B}_{13}$ , G1- $\text{Co}_{68}\text{Cu}_{23}\text{B}_9$  and G2- $\text{Fe}_{64}\text{Nb}_{28}\text{B}_8$ .

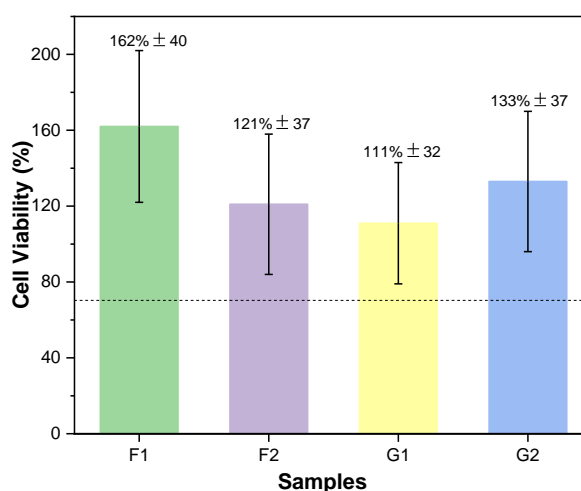


**Figure 8.** Illustration of the percentage of cell viability obtained for each sample analyzed (F1- $\text{Co}_{69}\text{Nb}_{23}\text{B}_8$ , F2- $\text{Fe}_{78}\text{Si}_9\text{B}_{13}$ , G1- $\text{Co}_{68}\text{Cu}_{23}\text{B}_9$  e G2- $\text{Fe}_{64}\text{Nb}_{28}\text{B}_8$ ), with the dotted line

representing the limiting value of 70% which, according to ISO 10993-5, is the minimum acceptable value for the biomaterial to be non-cytotoxic.

It can be seen that the samples presented cell viability above 70% as specified in the BS EN ISO 10993-5:2009 standard, although their variability is high and the minimum value is slightly below that specified, with emphasis on the samples decoded as F1-Co<sub>69</sub>Nb<sub>23</sub>B<sub>8</sub> and G2-Fe<sub>64</sub>Nb<sub>28</sub>B<sub>8</sub>, which were those with the highest cell viability, respectively.

However, all of them showed signs of having promising potential for applicability as metallic biomaterial for bone tissue regeneration and temporary implants for orthopedics. Based on the statistical analysis of the results obtained by the ANOVA test applied to the cell viability data of samples F1-Co<sub>69</sub>Nb<sub>23</sub>B<sub>8</sub>, F2-Fe<sub>78</sub>Si<sub>9</sub>B<sub>13</sub>, G1-Co<sub>68</sub>Cu<sub>23</sub>B<sub>9</sub> and G2-Fe<sub>64</sub>Nb<sub>28</sub>B<sub>8</sub>, we can infer that the calculated F statistic was approximately 0.100, while the associated p-value was approximately 0.956. This indicates that the F statistic is very low compared to the critical value of the F distribution for a significance level of 0.05, and the p-value is greater than the chosen significance level. Therefore, there is insufficient statistical evidence to reject the null hypothesis that the cell viability means of the groups F1-Co<sub>69</sub>Nb<sub>23</sub>B<sub>8</sub>, F2-Fe<sub>78</sub>Si<sub>9</sub>B<sub>13</sub>, G1-Co<sub>68</sub>Cu<sub>23</sub>B<sub>9</sub> and G2-Fe<sub>64</sub>Nb<sub>28</sub>B<sub>8</sub> are equal.

When we look at the distribution of variation in the data, we see that most of the variability is within groups (SSE = 17528.5), while the variability between groups is relatively low (SSG = 1317.375). This is consistent with the low F-statistic observed. The between-group degrees of freedom (df<sub>between</sub>) are 3, indicating that we are comparing the means of three different groups, while the within-group degrees of freedom (df<sub>within</sub>) are 4, indicating that the amount of data within each group is being considered.

The between-group (MSB) and within-group (MSW) mean squares assess the variability between and within groups, respectively. With MSB around 439.125 and MSW around 4382.125, the F-ratio close to 0.1 indicates that the variability between groups is lower than that within groups. Thus, there is no significant difference between the means of groups F1-Co<sub>69</sub>Nb<sub>23</sub>B<sub>8</sub>, F2-Fe<sub>78</sub>Si<sub>9</sub>B<sub>13</sub>, G1-Co<sub>68</sub>Cu<sub>23</sub>B<sub>9</sub> and G2-Fe<sub>64</sub>Nb<sub>28</sub>B<sub>8</sub>. It is concluded that the different titanium alloys did not have a significant impact on cell viability according to the data and methodology used.

As expected, and widely disseminated in the literature, the cytocompatibility of metal alloys, such results demonstrate, is in agreement with studies by Thanka Rajan et al. (2019) in which the viability of SaOS-2 cells was validated, which was greater than 100% for all dilutions, even at the 100% concentration of extracts coated with TFMG. The control (uncoated Ti6Al4V) showed lower viability than the specimen coated with TFMG [88].

In contrast, when compared with a study in which, despite the sample not being considered cytotoxic, only 78% cell viability was observed, and even after 48h of cell culture [89]. A new decrease in the proliferation rate (73%) is recorded after 72h. This suggests that the cells appeared to be very sensitive on the surface of Zr<sub>37</sub>Co<sub>34</sub>Cu<sub>20</sub>Ti<sub>9</sub> MG and require more time to record a constant increase in the number of viable cells [90].

In this regard, that corrosive species within the human physiological environment activate the thermodynamic corrosion tendencies of metallic materials [91,92]. Depending on the toxic nature of the released cations, several biological factors can be activated, which introduce inflammatory cascades and cell apoptosis. In this context, the new amorphous titanium-based alloy Ti<sub>44</sub>Zr<sub>10</sub>Pd<sub>10</sub>Cu<sub>6+x</sub>Co<sub>23-x</sub>Ta<sub>7</sub> (x = 0, 4, 8) showed biocompatibility characteristics with osteoblast-like cells (SaOS-2) that demonstrated excellent results for potential development of biomedical applications [93].

For comparison and example, evaluated the amorphous alloy based on Mg-Zn-Ca synthesized by mechanical grinding and used the MTT assay with MC3T3 osteoblastic cells and showed that the amorphous powder extract Mg<sub>60</sub>Zn<sub>35</sub>Ca<sub>5</sub> presented low cytotoxicity in relation to the MC3T3 cells tested, demonstrating great application as a promising biomaterial in orthopedic implants [94].

On the other hand, found in the release of metal ions such as  $Zn^{2+}$  and  $Mg^{2+}$  the induction of angiogenesis and cell proliferation, in addition to attenuated pro-inflammatory responses, which suggests a significant viability for such in the extracts studied with the release of ions that are conducive to the induction and viability of cell growth [95-100].

Although the results mentioned above in this thesis demonstrate that cell viability was around 70%, as specified in the BS EN ISO 10993-5:2009 standard, presenting it as a promising metallic biomaterial with potential for bone tissue regeneration and temporary orthopedic implants. This result can be corroborated by the studies when they characterized crystallized and relaxed amorphous Mg-Zn-Ca alloy tapes for application in bone regeneration, as well as in the biomedical orthopedics area [101-103].

The Materials and Methods should be described with sufficient details to allow others to replicate and build on the published results. Please note that the publication of your manuscript implicates that you must make all materials, data, computer code, and protocols associated with the publication available to readers. Please disclose at the submission stage any restrictions on the availability of materials or information. New methods and protocols should be described in detail while well-established methods can be briefly described and appropriately cited.

**Conflicts of Interest:** The authors declare no conflict of interest.

## References:

1. ABID, M. A.; ABID, D. A.; AZIZ, W. J.; RASHID, T. M. Iron oxide nanoparticles synthesized using garlic and onion peel extracts rapidly degrade methylene blue dye. *Physica B: Condensed Matter* **622**, p. 413277, 2021.
2. ADEJUYIGBE, B.; KALLINI, J.; CHIOU, D.; KALLINI, J. R. Osteoporosis: molecular pathology, diagnostics, and therapeutics. *International Journal of Molecular Sciences* **24(19)**, p. 14583, 2023.
3. ADELFA, R.; MIRZADEH, H.; ATAIE, A.; MALEKAN, M. Crystallization kinetics of mechanically alloyed amorphous Fe-Ti alloys during annealing. *Advanced Powder Technology* **31(8)**, p. 3215-3221, 2020.
4. AHANGARAN, F.; HASSANZADEH, A.; NOURI, S. Surface modification of  $Fe_3O_4@SiO_2$  microsphere by silane coupling agent. *International Nano Letters* **3**, p. 1–5, 2013.
5. AHMAD, M.; CHEN, J.; YANG, K.; SHAH, T.; ZHANG, Q.; ZHANG, B. Preparation of amidoxime modified porous organic polymer flowers for selective uranium recovery from seawater. *Chemical Engineering Journal* **418**, p. 129370, 2021.
6. ALOTHMAN, Z. A. A review: fundamental aspects of silicate mesoporous materials. *Materials* **5(12)**, p. 2874-2902, 2012.
7. AN, S.; GONG, Q.; HUANG, Y. Promotive Effect of Zinc Ions on the Vitality, Migration, and Osteogenic Differentiation of Human Dental Pulp Cells. *Biological Trace Element Research* **175(1)**, p. 112-121, 2017.
8. AN, Z. Y.; ZHANG, Y. H.; LI, X.; GU, Y. Magnetic and thermal characterization of Fe-B-P amorphous nanoparticles prepared by chemical reduction. *Journal of Magnetism and Magnetic Materials* **560**, p. 169648, 2022.
9. AVAR, B.; OZCAN, S. Characterization and amorphous phase formation of mechanically alloyed  $Co_{66}Fe_5Ni_5Ti_{25}B_5$  powders. *Journal of Alloys and Compounds* **650**, p. 53–58, 2015.

10. BAI, G.; DONG, H.; ZHAO, Z.; WANG, Y.; CHEN, Q.; QIU, M. Preparation of nanoscale Ni–B amorphous alloys and their application in the Selective Hydrogenation of Cinnamic Acid. *Journal of Nanoscience and Nanotechnology* **13(7)**, p. 5012-5016, 2013.
11. BECK, R. T.; ILLINGWORTH, K. D.; SALEH, K. J. Review of periprosthetic osteolysis in total joint arthroplasty: an emphasis on host factors and future directions. *Journal of Orthopaedic Research* **30 (4)**, p. 541-546, 2012.
12. BELDJEHEM, M.; ALLEG, S.; BENSEBAA, N.; SUÑOL, J. J.; GRENECHE, J. M. Thermal Stability, Structure, Hyperfine, and Magnetic Properties of Nanostructured FeCo-2.5 wt.% Ni Powders. *Journal of Superconductivity and Novel Magnetism* **36(1)**, p. 301-314, 2023.
13. BELYANSKY, M.; TRENARY, M. Reflection adsorption infrared spectroscopy of the oxidation of thin films of boron and hafnium diboride grown on Hf(0001). *Journal of Vacuum Science & Technology A: Vacuum, Surfaces, and Films* **15(6)**, p. 3065-3068, 1997.
14. BOSE, S.; KE, D.; SAHASRABUDHE, H.; BANDYOPADHYAY, A. Additive manufacturing of biomaterials. *Progress in Materials Science* **93**, p. 45-111, 2018.
15. BRUNOLD, T. C.; TAMURA, N.; KITAJIMA, N.; MORO-OKA, Y.; SOLOMON, E. I. Spectroscopic Study of  $[\text{Fe}_2(\text{O}_2)(\text{OBz})_2\{\text{HB}(\text{pz}^-)_3\}_2]$ : Nature of the  $\mu$ -1,2 Peroxide–Fe (III) Bond and Its Possible Relevance to  $\text{O}_2$  Activation by Non-Heme Iron Enzymes. *Journal of the American Chemical Society* **120(23)**, p. 5674-5690, 1998.
16. BURCHAM, L. J.; DATKA, J.; WACHS, I. E. In situ vibrational spectroscopy studies of supported niobium oxide catalysts. *The Journal of Physical Chemistry B* **103(29)**, p. 6015-6024, 1999.
17. CAO, Q.; HUANG, G.; MA, L.; XING, L. Comparison of a cold-sprayed and plasma-sprayed  $\text{Fe}_{25}\text{Cr}_{20}\text{Mo}_1\text{Si}$  amorphous alloy coatings on 40Cr substrates. *Materials and Corrosion* **71(11)**, p. 1872-1884, 2020.
18. CHEUNG, T.; BHARGAVA, S. K.; HOBDAV, M.; FOGER, K. Adsorption of NO on Cu exchanged zeolites, an FTIR study: effects of Cu levels, NO pressure, and catalyst pretreatment. *Journal of Catalysis* **158(1)**, p.301-310, 1996.
19. CHOI, K.; OMANOVIC, S. Solution combustion synthesis of nanostructured Ni/W-containing electrocatalysts for hydrogen evolution reaction: The effect of fuel-to-oxidant ratio. *Nano-Structures & Nano-Objects* **37**, p. 101075, 2024.
20. CHONG, K.; GAO, Y.; ZHANG, Z.; ZOU, Y.; LIANG, X. Thermal stability and corrosion behavior of a novel  $\text{Zr}_{22.5}\text{Ti}_{22.5}\text{Hf}_{22.5}\text{Ni}_{22.5}\text{Ta}_{10}$  high-entropy amorphous alloy. *Corrosion Science* **213**, p. 110979, 2023.
21. CUI, C.; REN, C.; LIU, Y.; WANG, S.; SU, H. Directional solidification of Fe–Al–Ta eutectic by electron beam floating zone melting. *Journal of Alloys and Compounds* **785**, p. 62-71, 2019.
22. DATTA, M. K.; CHOU, D. T.; HONG, D.; SAHA, P.; CHUNG, S. J.; LEE, B.; SIRINTERLIKCI, A.; RAMANATHAN, M.; ROY, A.; KUMTA, P. N. Structure and thermal stability of biodegradable Mg–Zn–Ca based amorphous alloys synthesized by mechanical alloying. *Materials Science and Engineering: B*: **176(20)**, p. 1637-1643, 2011.

23. DENG, J. F.; LI, H.; WANG, W. Progress in design of new amorphous alloy catalysts. *Catalysis today* **51(1)**, p. 113-125, 1999.
24. DONG, B.; ZHOU, S.; PAN, S.; WANG, Y.; QIN, J.; XING, Y. Relationship between relaxation embrittlement and atomic cluster structure in amorphous alloys. *Journal of Non-Crystalline Solids* **626**, p.122770, 2024.
25. FEIZABAD, M. H. K.; KHAYATI, G. R.; SHARAFI, S.; RANJBAR, M. Improvement of soft magnetic properties of Fe<sub>0.7</sub>Nb<sub>0.1</sub>Zr<sub>0.1</sub>Ti<sub>0.1</sub> amorphous alloy: A kinetic study approach. *Journal of Non-Crystalline Solids* **493**, p. 11-19, 2018.
26. FÜREDI, M.; MANZANO, C. V.; MARTON, A.; FODOR, B.; ALVAREZ-FERNANDEZ, A.; GULDIN, S. Beyond the meso/macroporous boundary: extending capillary condensation-based pore size characterization in thin films through tailored Adsorptives. *The Journal of Physical Chemistry Letters* **15(5)**, p. 1420-1427, 2024.
27. GALIMZYANOV, B. N.; MOKSHIN, A. V. Mechanical response of mesoporous amorphous NiTi alloy to external deformations. *International Journal of Solids and Structures* **224**, p. 111047, 2021.
28. GEORGEANU, V. A.; GINGU, O.; ANTONIAC, I. V.; MANOLEA, H. O. Current options and future perspectives on bone graft and biomaterials substitutes for bone repair, from clinical needs to advanced biomaterials research. *Applied Sciences* **13(14)**, p. 8471, 2023.
29. GÜLER, O.; VAROL, T.; ALVER, Ü.; ÇANAKÇI, A. The effect of flake-like morphology on the coating properties of silver coated copper particles fabricated by electroless plating. *Journal of Alloys and Compounds* **782**, p. 679-688, 2019.
30. GUO, X. X.; HU, T. T.; MENG, B.; SUN, Y.; HAN, Y. F. Catalytic degradation of anthraquinones-containing H<sub>2</sub>O<sub>2</sub> production effluent over layered Co-Cu hydroxides: defects facilitating hydroxyl radical generation. *Applied Catalysis B: Environmental* **260**, p. 118157, 2020.
31. HADJIIVANOV, K. I.; PANAYOTOV, D. A.; MIHAYLOV, M. Y.; IVANOVA, E. Z.; CHAKAROVA, K. K.; AN-DONOVA, S. M.; DRENCEV, N. L. Power of infrared and raman spectroscopies to characterize metal-organic frameworks and investigate their interaction with guest molecules. *Chemical Reviews* **121(3)**, p. 1286-1424, 2020.
32. HADJIIVANOV, K.; TSYNTSARSKI, B.; VENKOV, T.; KLISSURSKI, D.; DATURI, M., SAUSSEY, J.; LAVALLEY, J. C. FTIR spectroscopic study of CO adsorption on Co-ZSM-5: Evidence of formation of Co<sup>+</sup>(CO)<sub>4</sub> species. *Physical Chemistry Chemical Physics* **5(8)**, p. 1695-1702, 2003.
33. HOUSSOU, A.; AMIRAT, S.; FERKOUS, H.; ALLEG, S.; DADDA, K.; BOULECHFAR, R.; ERTO, A.; EL-BOUGHDIRI, N.; YADAV, K. K.; ALRESHIDI, M.A.; BHUTTO, J.K.; BOUCHELACHEM, W.; ABADLIA, L.; BENGUERBA, Y. Experimental and computational investigations on mechanically alloyed Fe<sub>55</sub>Co<sub>30</sub>Ni<sub>15</sub> powders. *Powder Technology*, p. 119203, 2023.

34. HUANG, L. J.; LIN, H. J.; WANG, H.; OUYANG, L. Z.; ZHU, M. Amorphous alloys for hydrogen storage. *Journal of Alloys and Compounds* **941**, p. 168945, 2023.
35. HUANG, S. J.; MUNEEB, A.; ABBAS, A.; SANKAR, R. The effect of Mg content and milling time on the solid solubility and microstructure of Ti–Mg alloys processed by mechanical milling. *Journal of Materials Research and Technology* **11**, p. 1424-1433, 2021.
36. IRWANSYAH, F. S.; AMAL, A. I.; DIYANTHI, E. W.; HADISANTOSO, E. P.; NOVIYANTI, A. R.; EDDY, D. R.; RISDIANA, R. How to read and determine the specific surface area of inorganic materials using the Brunauer-Emmett-Teller (BET) method. *ASEAN Journal of Science and Engineering* **4(1)**, p. 61-70, 2024.
37. **ISO 10993-5:2009 Biological evaluation of medical devices Part 5: Tests for in vitro cytotoxicity.** ISO Standards 2009.
38. **ISO. Biological evaluation of medical devices. Tests for in vitro cytotoxicity.**: International Organization for Standardization, BS EN ISO 10993-5, 2009.
39. JABED, A.; RAHMAN, Z. U.; KHAN, M. M.; HAIDER, W.; SHABIB, I. Combinatorial development and in vitro characterization of the quaternary Zr–Ti–X–Y (X–Y= Cu–Ag/Co–Ni) metallic glass for prospective bioimplants. *Advanced Engineering Materials* **21(12)**, p. 1900726, 2019.
40. JEŽ, B.; NABIALEK, M.; JEŽ, K. J. Preparation of Magnetic Composites Based on Bulk Amorphous Iron Alloys. *Materiale Plastice* **56(4)**, p. 1008, 2019.
41. KANEKO, K.; OTSUKA, H. New IUPAC recommendation and characterization of nanoporous materials with physical adsorption. *Accounts of Materials & Surface Research* **5(2)**, p. 25-32, 2020.
42. KHITOUNI, N.; HAMMAMI, B.; LLORCA-ISERN, N.; MBAREK, W. B.; SUÑOL, J. J.; KHITOUNI, M. Microstructure and Magnetic Properties of Nanocrystalline Fe<sub>60-x</sub>Co<sub>25</sub>Ni<sub>15</sub>Si<sub>x</sub> Alloy Elaborated by High-Energy Mechanical Milling. *Materials* **15 (18)**, p. 6483, 2022.
43. KOONS, G. L.; DIBA, M.; MIKOS, A. G. Materials design for bone-tissue engineering. *Nature Reviews Materials* **5(8)**, p. 584-603, 2020.
44. KOWALSKI, P. S.; BHATTACHARYA, C.; AFEWERKI, S.; LANGER, R. Smart biomaterials: recent advances and future directions. *ACS Biomaterials Science & Engineering* **4(11)**, p. 3809-3817, 2018.
45. LAMPLOT, J. D.; SMITH, B. L.; SLONE, H. S.; HAUCK, O. L.; WIJICKS, C. A. Tape-reinforced graft suturing and retensioning of adjustable-loop cortical buttons improve quadriceps tendon autograft biomechanics in anterior cruciate ligament reconstruction: A cadaveric study. *Arthroscopy: The Journal of Arthroscopic & Related Surgery* **40(1)**, p.136-145, 2024.
46. LEE, J. D. *Química inorgânica Não Tão Concisa*. São Paulo: Editora Blücher, 1999, 544p.

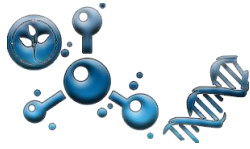
47. LEE, T.; YAMASAKI, M.; KAWAMURA, Y.; LEE, Y.; LEE, C. S. High strain-rate superplasticity of AZ91 alloy achieved by rapidly solidified flaky powder metallurgy. *Materials Letters* **234**, p. 245-248, 2019.
48. LI, R.; CHEN, Q.; JI, L.; PENG, X.; HUANG, G. Based on internal friction theory: Investigating of Fe-based bulk amorphous alloys on mechanical properties with different Si content. *Journal of Non-Crystalline Solids* **563**, p. 120813, 2021.
49. LIU, K.; WANG, S.; FENG, Y.; ZHANG, K.; ZHANG, Y. Phase transformation mechanism and magnetic properties of Sm-Fe alloys produced by melt-spinning and high-energy ball milling. *Journal of Magnetism and Magnetic Materials* **513**, p. 167229, 2020.
50. LIU, L.; AHMADI, Y.; KIM, K. H.; KUKKAR, D.; SZULEJKO, J. E. The relative dominance of surface oxygen content over pore properties in controlling adsorption and retrograde behavior of gaseous toluene over microporous carbon. *Science of The Total Environment* **906**, p. 167308, 2024.
51. LIU, N.; GAO, Y.; CHEN, C.; ZHOU, P.; WANG, X.; ZHANG, J.; CAO, J. Oxidation behavior of  $\text{Al}_{15}\text{Fe}_{20}\text{Co}_{20}\text{Ni}_{20}\text{Cr}_{25-x}\text{Nb}_x$  high-entropy alloys at elevated temperatures. *Vacuum* **213**, p. 112092, 2023.
52. LIU, S.; SHOHJI, I.; KOBAYASHI, T.; HIROHASHI, J.; WAKE, T.; YAMAMOTO, H.; KAMAKOSHI, Y. Mechanistic study of Ni–Cr–P alloy electrodeposition and characterization of deposits. *Journal of Electroanalytical Chemistry* **897**, p. 115582, 2021.
53. LIU, X.; WANG, X.; SI, Y.; HAN, F. Glass-Forming Ability and Thermal Properties of  $\text{Al}_{70}\text{Fe}_{12.5}\text{V}_{12.5}\text{X}_5$  (X= Zr, Nb, Ni) Amorphous Alloys via Minor Alloying Additions. *Nanomaterials* **11(2)**, p. 488, 2021.
54. LOPEZ, J. A.; GONZÁLEZ, F.; BONILLA, F. A.; ZAMBRANO, G.; GÓMEZ, M. E. Synthesis and characterization of Fe<sub>3</sub>O<sub>4</sub> magnetic nanofluid. *Revista Latinoamericana de Metalurgia y Materiales* **30(1)**, p. 60-66, 2010.
55. MÁLEK, J. Structural relaxation rate and aging in amorphous solids. *The Journal of Physical Chemistry C*:**127(12)**, p. 6080-6087, 2023.
56. MANOJ, J.; VIZHI, R. E. Effect of Al substitution on their structural and magnetic properties of  $\text{Ba}_{0.5}\text{Sr}_{0.5}\text{Fe}_{12}\text{O}_{19}$  prepared via sol–gel auto-combustion method. *Journal of Materials Science: Materials in Electronics* **35(6)**, p. 370, 2024.
57. MONAVARIAN, M.; KADER, S.; MOEINZADEH, S.; JABBARI, E. Regenerative scar-free skin wound healing. *Tissue Engineering Part B: Reviews* **25(4)**, p.294-311, 2019.
58. MONETA, M.; WASIAK, M.; SOVAK, P. Temperature dependence of structural and magnetic transformations in Fine-met-type amorphous alloys with Fe substituted for La. *Journal of Thermal Analysis and Calorimetry***148(4)**, p. 1577-1580, 2023.

59. MONFARED, A.; GHAEI, A.; EBRAHIMI-BAROUGH, S. Preparation and characterization of crystallized and relaxed amorphous Mg-Zn-Ca alloy ribbons for nerve regeneration application. *Journal of Non-Crystalline Solids* **489**, p. 71-76, 2018.
60. MOOSAVINEJAD, S. M.; MADHOUSHI, M.; VAKILI, M.; RASOULI, D. Evaluation of degradation in chemical compounds of wood in historical buildings using FT-IR and FT-Raman vibrational spectroscopy. *Maderas. Ciencia y Tecnología* **21(3)**, p. 381-392, 2019.
61. MSETRA, Z.; KHITOUNI, N.; ALSAWI, A.; KHITOUNI, M.; OPTASANU, V.; SUÑOL, J. J.; CHEMINGUI, M. Structural, microstructural, and magnetic properties of nanocrystalline-amorphous Fe–Co–Ta–B alloy processed by high-energy mechanical alloying. *Journal of Materials Research and Technology* **26**, p. 8934-8943, 2023.
62. MUKHTAR, A.; MELLON, N.; SAQIB, S.; LEE, S. P.; BUSTAM, M. A. Extension of BET theory to CO<sub>2</sub> adsorption isotherms for ultra-microporosity of covalent organic polymers. *SN Applied Sciences* **2(7)**, p. 1-4, 2020.
63. MURPHY, N. J.; GRAAN, D.; BRIGGS, G. D.; BALOGH, Z. J. Acute minimally invasive bone grafting of long bone fractures to reduce the incidence of fracture non-union. *Medical Hypotheses* **178**, p. 111131, 2023.
64. MURUGAIYAN, P.; MITRA, A.; ROY, R. K.; PANDA, A. K. Nanocrystallization and Core-loss properties of Fe-rich FeSiBPNbCu nanocrystalline alloy. *Journal of Magnetism and Magnetic Materials* **552**, p. 169228, 2022.
65. NWAHARA, N.; ABRAHAMS, G.; MACK, J.; PRINSLOO, E.; NYOKONG, T. A hypoxia responsive silicon phthalocyanine containing naphthoquinone axial ligands for photodynamic therapy activity. *Journal of Inorganic Biochemistry* **239**, p. 112078, 2023.
66. NYKYRUY, Y.; MUDRY, S.; KULYK, Y.; BORISYUK, A. Magnetic properties and nanocrystallization process in Co–(Me)–Si–B amorphous ribbons. *Applied Nanoscience*, p. 1-11, 2022.
67. PETIT, L.; CARDINAL, T.; VIDEAU, J. J.; DURAND, E.; CANIONI, L.; MARTINES, M.; GUYOT, Y.; BOULON, G. Effect of niobium oxide introduction on erbium luminescence in borophosphate glasses. *Optical Materials* **28(3)**, p. 172-180, 2006.
68. PRABHU, Y.; JAIN, A.; VINCENT, S.; RYU, W. H.; PARK, E. S.; KUMAR, R.; BAGDE, A. D.; BHATT, J. Compositional design and in vitro investigation on novel Zr–Co–Cu–Ti metallic glass for biomedical applications. *Intermetallics* **150**, p. 107692, 2022.
69. PRIEZJEV, N. V. The effect of thermal history on the atomic structure and mechanical properties of amorphous alloys. *Computational Materials Science* **174**, p. 109477, 2020.
70. PRIMEAU, N.; VAUTEY, C.; LANGLET, M. The effect of thermal annealing on aerosol-gel deposited SiO<sub>2</sub> films: a FTIR deconvolution study. *Thin Solid Films* **310(1-2)**, p. 47-56, 1997.

71. PUTRA, N. E.; MIRZAALI, M. J.; APACHITEI, I.; ZHOU, J.; ZADPOOR, A. A. Multi-material additive manufacturing technologies for Ti-, Mg-, and Fe-based biomaterials for bone substitution. *Acta biomaterialia* **109**, p. 1-20, 2020.
72. RAJAN, S. THANKA; BENDAVID, A.; SUBRAMANIAN, B. Cytocompatibility assessment of Ti-Nb-Zr-Si thin film metallic glasses with enhanced osteoblast differentiation for biomedical applications. *Colloids and Surfaces B: Biointerfaces* **173**, p. 109-120, 2019.
73. RASOULI, A.; NAFFAKH-MOOSAVY, H. Dissimilar laser welding of NiTi shape memory alloy to NiCr alloy. *Journal of Materials Research and Technology* **26**, p. 3947-3956, 2023.
74. RATHI, A.; MEKA, V. M.; JAYARAMAN, T. V. Synthesis of nanocrystalline equiatomic nickel-cobalt-iron alloy powders by mechanical alloying and their structural and magnetic characterization. *Journal of Magnetism and Magnetic Materials* **469**, p. 467-482, 2019.
75. RATHOD, V.; ANUPAMA, A. V.; KUMAR, R. V.; JALI, V. M.; SAHOO, B. Correlated vibrations of the tetrahedral and octahedral complexes and splitting of the absorption bands in FTIR spectra of Li-Zn ferrites. *Vibrational Spectroscopy* **92**, p. 267-272, 2017.
76. ROESNER, M.; ZANKOVIC, S.; KOVACS, A.; BENNER, M.; BARKHOFF, R.; SEIDENSTUECKER, M. Mechanical Properties and Corrosion Rate of ZnAg<sub>3</sub> as a Novel Bioabsorbable Material for Osteosynthesis. *Journal of Functional Biomaterials* **15** (2), p. 28, 2024.
77. ROOHANI, I.; YEO, G. C.; MITHIEUX, S. M.; WEISS, A. S. Emerging concepts in bone repair and the premise of soft materials. *Current Opinion in Biotechnology* **74**, p. 220-229, 2022.
78. SAHU, P.; SAMAL, S.; KUMAR, V. Influence of Si and Mn on the Phase Formation, Crystallization Kinetics, and Enhanced Magnetic Properties of Mechanically Alloyed NiCoFe (SiMn)<sub>x</sub> High Entropy Amorphous Alloys. *Silicon*, p. 1-26, 2023.
79. SALWA, P.; GORYCZKA, T. Crystallization of mechanically alloyed Ni<sub>50</sub>Ti<sub>50</sub> and Ti<sub>50</sub>Ni<sub>25</sub>Cu<sub>25</sub> shape memory alloys. *Journal of Materials Engineering and Performance* **29**(5), p. 2848-2852, 2020.
80. SANDITOV, D. S.; OJOVAN, M. I.; DARMAEV, M. V. Glass transition criterion and plastic deformation of glass. *Physica B: Condensed Matter* **582**, p. 411914, 2020.
81. SERAFIN, J.; DZIEJARSKI, B. Activated carbons—Preparation, characterization and their application in CO<sub>2</sub> capture: A review. *Environmental Science and Pollution Research* **31**(28), p. 40008-40062, 2024.
82. SHAN, L.; WANG, X.; WANG, Y. Extension of solid solubility and structural evolution in nano-structured Cu-Cr solid solution induced by high-energy milling. *Materials* **13**(23), p. 5532, 2020.

83. SHEN, J. F.; WU, C. M.; YU, J. J.; LI, Y. R. Investigation on molecular cluster behavior and initiation of capillary condensation within nanoarrays. *International Journal of Heat and Mass Transfer* **210**, p. 124173, 2023.
84. SHI, X. Z.; GU, Y.; LIU, T. Y.; JIANG, Z. H.; LI, R.; ZENG, F. Effect of different P<sub>2</sub>O<sub>5</sub>/SnF<sub>2</sub> ratios on the structure and properties of phosphate glass. *Journal of Non-Crystalline Solids* **578**, p. 121350, 2022.
85. ŠPALDOŇOVÁ, A.; HAVELCOVÁ, M.; LAPČÁK, L.; MACHOVIČ, V.; TITĚRA, D. Analysis of beeswax adulteration with paraffin using GC/MS, FTIR-ATR and Raman spectroscopy. *Journal of Apicultural Research* **60(1)**, p. 73-83, 2021.
86. SUN, C.; HAI, X.; XI, S.; FAN, Z.; LI, P.; WANG, W. New insights of solid-state alloying and amorphous-nanocrystalline cyclic phase transitions during Cr-40 wt.% Mo powder milling. *Journal of Alloys and Compounds* **731**, p. 667-677, 2018.
87. TANTAVISUT, S.; LOHWONGWATANA, B.; KHAMKONGKAEAO, A.; TANAVALLEE, A.; TANGPORNPRASERT, P.; ITTIRAVIVONG, P. In vitro biocompatibility of novel titanium-based amorphous alloy thin film in human osteoblast-like cells. *Chulalongkorn Medical Journal* **63(2)**, p. 89-93, 2019.
88. TAO, X.; ZHANG, Z.; ZHANG, B.; ZHU, S.; FAN, Y.; TIAN, H. Plasma sprayed CoNiCrMoNb (BSi) high-entropy amorphous alloy coating: The effect of spraying power on microstructure, mechanical and tribological properties. *Materials Chemistry and Physics* **314**, p. 128887, 2024.
89. THANKA RAJAN, S.; BENDAVID, A.; SUBRAMANIAN, B. Cytocompatibility assessment of Ti-Nb-Zr-Si thin film metallic glasses with enhanced osteoblast differentiation for biomedical applications. *Colloids and Surfaces B: Biointerfaces* **173**, p. 109-120, 2019.
90. TIAN, Q.; DENG, K.; XU, Z.; HAN, K.; ZHENG, H. Microstructural Characterization and Mechanical Property of Al-Li Plate Produced by Centrifugal Casting Method. *Metals* **11(6)**, p. 966, 2021.
91. TIAN, Y.; CHEN, Q.; YAN, C.; DENG, H.; HE, Y. Classification of adsorption isotherm curves for shale based on pore structure. *Petrophysics* **61(05)**, p. 417-433, 2020.
92. TONCÓN-LEAL, C. F.; VILLARROEL-ROCHA, J.; SILVA, M. T. P. D.; BRAGA, T. P.; SAPAG, K. Characterization of mesoporous region by the scanning of the hysteresis loop in adsorption-desorption isotherms. *Adsorption* **27(7)**, p. 1109-1122, 2021.
93. VASIĆ, M. M.; ŽÁK, T.; PIZÚROVÁ, N.; SIMATOVIĆ, I. S.; MINIĆ, D. M. Influence of Thermal Treatment on Microstructure and Corrosion Behavior of Amorphous Fe<sub>40</sub>Ni<sub>40</sub>B<sub>12</sub>Si<sub>8</sub> Alloy. *Metallurgical and Materials Transactions A*: **52**, p. 34-45, 2021.
94. VELMURUGAN, C.; SENTHILKUMAR, V. The effect of Cu addition on the morphological, structural and mechanical characteristics of nanocrystalline NiTi shape memory alloys. *Journal of Alloys and Compounds* **767**, p. 944-954, 2018.
95. WANG, J. L.; WAN, Y.; MA, Z. J.; GUO, Y. C.; YANG, Z.; WANG, P.; LI, J. P. Glass-forming ability and corrosion performance of Mn-doped Mg-Zn-Ca amorphous alloys for biomedical applications. *Rare Metals* **37(7)**, p. 579-586, 2018.

96. WANG, N.; CAO, Q.; WANG, X.; DING, S.; ZHANG, D.; JIANG, J. Z. Ultra-strong and ductile amorphous-crystalline Ti-Zr-Hf-Nb-Ta/Co-Ni-V nanolaminate thin films. *Journal of Alloys and Compounds* **973**, 172874, 2024.
97. WANG, S.; XU, T.; WU, Y.; CHEN, X.; YANG, X. Brazing Temperature Effects on the Microstructure and Mechanical Properties of Ti-45Al-8Nb Joints Using TiZrCuNi Amorphous Interlayer. *Coatings* **14(3)**, p. 300,2024.
98. WANG, Z. H.; URISU, T.; WATANABE, H.; OOI, K.; RAO, G. R.; NANBU, S.; MAKI, M.; AOYAGI, M. Assignment of surface IR absorption spectra observed in the oxidation reactions:  $2\text{H}+\text{H}_2\text{O}/\text{Si}$  (1 0 0) and  $\text{H}_2\text{O}+\text{H}/\text{Si}$  (1 0 0). *Surface science* **575(3)**, p. 330-342, 2005.
99. WU, J.; CHENG, X.; WU, J.; CHEN, J.; PEI, X. The development of magnesium-based biomaterials in bone tissue engineering: A review. *Journal of Biomedical Materials Research Part B: Applied Biomaterials* **112(1)**, p.e35326, 2024.
100. YAYKASLI, H.; AVAR, B.; PANIGRAHI, M.; GOGEBAKAN, M.; ESKALEN, H. Investigation of the Microstructural, Morphological, and Magnetic Properties of Mechanically Alloyed  $\text{Co}_{60}\text{Fe}_{18}\text{Ti}_{18}\text{Si}_4$  Powders. *Arabian Journal for Science and Engineering* **48(1)**, p. 845-854, 2023.
101. YUAN, H.; ZHOU, L.; WANG, G. T.; ZHENG, L. B.; YANG, Y. Z. Si microalloying optimizes the thermal stability, crystallization behaviors and magnetic properties of Fe-rich Fe-B-Cu-Hf alloys. *Journal of Magnetism and Magnetic Materials* **500**, p. 166339, 2020.
102. ZHANG, Y.; LIU, Y.; ZHENG, R.; ZHENG, Y.; CHEN, L. Research progress on corrosion behaviors and biocompatibility of rare-earth magnesium alloys in vivo and in vitro. *Journal of Rare Earths* **4(12)**, p. 1827-1842, 2023.
103. ZHAO, Q.; GAO, C.; HOU, L.; YANG, H. Emerging Phosphate-Functionalized  $\text{Co}_3\text{O}_4/\text{Kaolinite}$  Composites for Enhanced Activation of Peroxymonosulfate. *Inorganic Chemistry* **62(12)**, p. 4823-4834, 2023.
104. HOU, L.; WANG, Q.; FAN, X.; MIAO, F.; YANG, W.; SHEN, B. Effect of Co addition on catalytic activity of FePCCu amorphous alloy for methylene blue degradation. *New Journal of Chemistry* **43(16)**, p. 6126-6135, 2019.



Type of the Paper (Editorial)

## Digital Dentistry: The Start of the Revolution

Rasha M. Abdelraouf <sup>1\*</sup>

<sup>1</sup> Biomaterials Department, Faculty of Dentistry, Cairo University, Cairo (11553), Egypt.

\* Corresponding author e-mail: [rasha.abdelraouf@dentistry.cu.edu.eg](mailto:rasha.abdelraouf@dentistry.cu.edu.eg)

**Citation:** Rasha M. Abdelraouf.

*Digital Dentistry: The Start of the Revolution*. *Biomat. J.*, 3 (1),54 – 55 (2024).

<https://doi.org/10.5281/znodo.5829408>

Received: 19 December 2024

Accepted: 20 December 2024

Published: 25 December 2024



**Copyright:** © 2022 by the authors. Submitted for possible open access publication under the terms and conditions of the Creative Commons Attribution (CC BY) license (<https://creativecommons.org/licenses/by/4.0/>).

**Abstract:** The digital revolution in dentistry is the future, not just a passing fad. With these developments, patients can anticipate receiving dental care that is more accurate, effective, and customized. As technology develops further, there are countless ways to improve your smile. Your next dental appointment may surprise you with how much more digital it has become.

**Keywords:** 3D Printing; intraoral scanners; artificial Intelligence; tele-dentistry; digital Smile; smart materials

The dentistry sector is undergoing a huge transition, especially to the digital revolution. Advanced technology are not only boosting the precision and efficiency of dental procedures but also transforming the patient experience. What does the digital era hold for your smile in the future?

### 1. Intraoral Scanners Revolution

We can now obtain 3D information for the implementation of a prosthetic Computer Assisted Design (CAD) project by performing an intraoral scan of one or more prosthetic preparations using powerful intraoral scanners. Using the modelling software, we can create our restoration, which will subsequently be milled in a highly aesthetic material (ceramic, lithium disilicate, zirconia) and applied to the patient. The same is true for implants; our patients have never liked the need to take traditional physical impressions using impression trays. Concurrently, bone-related data obtained by low-dose radiation Cone Beam Computed Tomography (CBCT) can be superimposed on data pertaining to teeth and gingiva obtained from an intraoral scan. Thus, using software to direct the procedure, it is possible to plan the ideal implant placement. A surgical template, which can be physically constructed using a variety of techniques and materials, receives planning data. By using this guide, the surgeon will be able to place the implants precisely without having to lift a flap.

### 2. Digital Revolution and 3D Printing

The days of making dental impressions using unpleasant molds are long gone. Your teeth can now be imaged with accuracy, speed, and comfort thanks to digital scanners. Dental labs that use 3D printing technology to create crowns, bridges, and other dental prosthesis can instantaneously access this data. A quicker turnaround time and a flawless fit are the outcomes, guaranteeing that your smile feels and looks natural. One of the most innovative advancements in digital dentistry is 3D printing. It makes it possible to produce dental prosthesis including crowns, bridges, and dentures quickly and accurately like never before. Because custom-fit devices can be created quickly and effectively, this technology decreases the amount of time patients spend in the chair and the number of visits needed.

### 3. AI-Powered Diagnostics and Treatment Planning

Artificial Intelligence (AI) is playing an increasingly crucial role in dentistry. AI-powered systems can analyze dental photos with astonishing precision, enabling dentists discover diseases like cavities, gum disease, and even oral tumors at an early stage.

Furthermore, by forecasting results and recommending the best course of action, AI helps with treatment planning. In dentistry, artificial intelligence (AI) is starting to revolutionize the game. Dental photos may be analyzed with remarkable accuracy by AI-powered diagnostic systems, which can spot problems that the human eye might overlook. Better results can also be achieved by using AI to help create personalized treatment plans based on each patient's particular oral health profile.

#### **4. Tele-dentistry**

As tele-dentistry has grown in popularity, patients can now consult with their dentists from a distance. Whether it's for a follow-up appointment, a consultation for a second opinion, or just advice on a dental concern, tele-dentistry offers convenience without compromising the quality of care, which is especially helpful for patients who live in remote areas or have mobility issues.

#### **5. Digital Smile Design**

A state-of-the-art method called Digital Smile Design (DSD) plans and visualizes your dental procedures using digital technology before they start. You can see a virtual representation of your new smile with DSD, which helps you decide on your course of treatment. This individualized approach guarantees that the outcome will precisely match your expectations.

#### **6. Smart Dental Devices**

In the field of oral care, wearable technology and smart dental gadgets are becoming more widespread. These advancements are enabling patients to take charge of their oral hygiene like never before, from smart toothbrushes that track your brushing habits and provide feedback to devices that check the health of your teeth and gums.

#### **7. Bioprinting and Regenerative Dentistry**

Going forward, regenerative dentistry and bioprinting have the potential to completely transform the way we provide dental care. While regenerative techniques may eventually allow for the regrowth of damaged or lost teeth, bioprinting may make it possible to create living tissues for dental repairs.